Technical Report
TR-21-11
September 2021

Radiolysis calculations of air, argon and water mixtures in a KBS-3 canister

Jim Henshaw
Kastriot Spahiu

SVENSK KÄRNBRÄNSLEHANTERING AB

SWEDISH NUCLEAR FUEL
AND WASTE MANAGEMENT CO

Box 3091, SE-169 03 Solna
Phone +46 8 459 84 00
skb.se

SVENSK KÄRNBRÄNSLEHANTERING

ISSN 1404-0344
SKB TR-21-11
ID 1942127
September 2021

Radiolysis calculations of air, argon and water mixtures in a KBS-3 canister

Jim Henshaw, Morson

Kastriot Spahiu, Svensk Kärnbränslehantering AB

Keywords: Radiolysis, Nitric acid, Ammonia, Corrosion.

This report is published on www.skb.se

Abstract

This report discusses the results of a gas phase radiolysis model developed to understand the conditions inside the KBS-3 canister. The model predicts the gas phase concentrations of potential aggressive species such as HNO_3, NH_3 and H_2O_2 produced from the radiolysis chemistry of Ar-air-water mixtures. Inside the canister corrosion of the steel surfaces is expected to occur, consuming O_2, H_2O and generating H_2, and the model also simulates these processes and their effect on the radiolysis chemistry. The model has been validated against laboratory radiation studies on Ar-air-water type mixtures and then applied to the KBS-3 canister. The results of all these calculations are discussed in this report.

Sammanfattning

Denna rapport presenterar resultat av modellering av radiolys i gasfas, vilken utvecklats för att förstå förhållandena inuti en KBS-3 kapsel. Modellen förutsäger koncentrationerna av potentiellt aggressiva molekyler som HNO_3, NH_3 och H_2O_2, vilka bildas på grund av radiolys av den blandning av argon, luft och vatten som förväntas inne kapseln. Eftersom det kommer finnas kolstål och segjärn i kapselns insats, är det förväntat att järnkorrosion kommer ske inne i kapseln. Denna korrosion förbrukar syrgas och vatten och genererar vätgas. Modellen simulerar dessa processer och deras effekt på radiolysreaktionerna. Modellen har validerats mot experimentella studier av strålningskemi i blandningar av argon, luft och vatten, och sedan har modellen använts för modellering av KBS-3-kapseln. Beräkningsresultaten diskuteras i denna rapport.

Contents

1 Introduction

The KBS-3 canister is designed to encapsulate spent nuclear fuel for geological disposal and was developed by SKB of Sweden (SKB 2010). The purpose of these canisters is to store both PWR and BWR fuel assemblies. The basic KBS-3 design consists of a copper overpack covering a carbon steel and cast-iron inner container[1], which is largely for structural support with the copper cover intended as the primary barrier to ingress of external ground water. The inner container is closed with a screw fitting lid with a gas seal to prevent gas transport into the gap between the inner container and the copper overpack. The lid of the copper overpack is sealed with friction stir welding.

It has been assumed that some water will be transferred into the canister along with the damaged fuel. It is also assumed that although the free gas volume within the canister is filled with argon, a small fraction of air will remain. The gas seal separating the fuel channels of the insert from the gap between the insert and the copper shell is not intended for long term service, hence it must be assumed that both container materials will be exposed to a H_2O-Ar-Air gas mixture. It is known that irradiation of moist air can lead to the production of aggressive reagents, such as nitric acid, that can cause stress corrosion cracking of the steels, (Marsh 1990). Should the gas phase inside the canister become chemically reducing, for example as a consequence of hydrogen production from both water radiolysis and steel corrosion, then another potential radiolysis product is ammonia, known to corrode copper (Marsh 1990). Important questions then are what chemical conditions will prevail inside the canister during the potential many centuries of storage, are species such as nitric acid and ammonia likely to be produced and if so, then how much is likely to form?

An early assessment of the gas phase conditions inside the Advanced Cold Process Canister (ACPC), an early version of the KBS-3 canister, was performed by Henshaw et al. (1990) and Henshaw (1994) using a model to simulate the gas phase radiolysis chemistry of moist air/Ar mixtures. This same chemistry model has also been used to examine a number of health physics issues relating to ozone formation in the location of linear accelerators (Endo et al. 1996, 1998). The model simulates the primary interactions of the radiation with the initial gaseous species present and the subsequent chemistry of the reactive primary species that leads to stable molecules, such as nitric acid and ammonia. The chemistry used in the Henshaw et al. (1990) and Henshaw (1994) models was not complete, as described below, and in addition the rate constants utilised in this earlier work are now over 25 years old. It was thought prudent therefore to improve the chemistry and update the rate constants used in these models. A new version of the moist air/Ar radiolysis model has therefore been created, which is described below. The Henshaw et al. (1990) and Henshaw (1994) work also assumed:

- At the presumed canister temperature all the water present was in the gaseous state, for small quantities this is correct but for larger quantities at lower temperatures it is not the case.
- That corrosion taking place in the system had no impact on the radiolysis chemistry. However, corrosion consumes O_2 and H_2O[2] and will generate H_2 which will have a significant impact on the gas phase chemistry.

The new model does not make these assumptions, the model accounts for the presence of liquid water which maintains the vapour at the saturation pressure. The model also accounts for the effect of corrosion on the gas phase chemistry.

Section 2 gives a brief description of moist air/Ar radiolysis chemistry describing what is different about the chemistry in the current model compared to that used by Henshaw et al. (1990) and Henshaw (1994). This section also describes the differential equations that are solved for this problem, including those used to account for evaporation and corrosion in the canister. Section 3 describes a number of validation calculations performed to test that the gas phase chemistry model provides reasonable results when compared with laboratory data. Section 4 describes the different initial canister conditions that are modelled here and presents the results of the calculations for these scenarios. Section 5 is a discussion of the results and Section 6 is the summary and conclusions.

[1] Both materials (cast iron and carbon steel) are components of the insert and are assumed to corrode with similar rates. The surfaces of fuel channels are carbon steel (relatively large surface), the same holds for the lid. The outer surface of the inner cylinder and the top and bottom surfaces are cast iron.

[2] It also consumes oxidising species produced from radiolysis, e.g. H_2O_2, but this is not considered in this study.

2 Radiolysis of moist air/argon mixtures – model description

2.1 Radiolysis chemistry

A set of reactions describing the radiation chemistry of moist air mixtures was first suggested by Person and Ham (1988) based on earlier work by Harteck and Dondes (1964) and Dmitriev (1965). A similar reaction scheme was also developed by Busi et al. (1987). This chemistry was developed in order to understand the potential of using electron beam irradiations to remove NO_X and SO_X emissions from flue gases of carbon burning power plants and large-scale smelters (Park et al. 2019). Here irradiation to produce nitric and sulphuric acid from gaseous NO_X and SO_X is beneficial as the acids can be efficiently scrubbed out using an alkaline solid/solution. Of course, in the case of the KBS-3 canister their production is deleterious due to their potential to cause stress corrosion cracking (Marsh 1990).

The primary interactions of radiation with N_2, O_2 and H_2O leads to the production of a range of free radicals and ionic species:

Primary reactions

$$N_2 \xrightarrow{Rad} N_2^+, N^+, e^-, N, N_2^* \quad (2\text{-}1)$$

$$H_2O \xrightarrow{Rad} H_2O^+, H^+, e^-, H, O, OH \quad (2\text{-}2)$$

$$O_2 \xrightarrow{Rad} O_2^+, O^+, e^-, O, O_2^* \quad (2\text{-}3)$$

and when Ar is present:

$$Ar \xrightarrow{Rad} Ar^+, Ar^*, e^- \quad (2\text{-}4)$$

Here O_2^* and Ar^* are excited electronic states of O_2 and Ar. Following these initial interactions, a complex sequence of reactions can then take place that includes:

Ion – ion, ion – molecule reactions

For example,

$$O_2^+ + NO_2^- \rightarrow O_2 + NO_2 \quad (2\text{-}5)$$

$$O_2^+ + NO \rightarrow O_2 + NO^+ \quad (2\text{-}6)$$

Many of these reactions lead to radical and molecular species, for example the reactions

$$N_2^+ + e^- \rightarrow 2N \quad (2\text{-}7)$$

$$N^+ + e^- \rightarrow N \quad (2\text{-}8)$$

$$N^+ + O_2 \rightarrow NO^+ + O \quad (2\text{-}9)$$

$$NO^+ + e^- \rightarrow NO + hv \quad (2\text{-}10)$$

give rise to N, O and NO.

Free radical – radical, radical-molecule reactions

The following example reactions lead to NO and NO_2 production:

$$N + O_2 \rightleftharpoons NO + O \quad (2\text{-}11)$$

$$N + OH \leftrightharpoons NO + H \quad (2\text{-}12)$$

$$NO + O + M \leftrightharpoons NO_2 + M \quad (2\text{-}13)$$

Reaction 2-12 is significantly faster than reaction 2-11 so the presence of water often speeds up the nitrogen oxidation process. OH is produced by the primary interactions of the radiation with water but another important pathway is via the formation of the $O_2H_2O^+$ cluster formed thus:

$$O_2^+ + H_2O + M \rightarrow O_2H_2O^+ + M \quad (2\text{-}14)$$

followed by

$$O_2H_2O^+ + H_2O \rightarrow H_3O^+ + OH + O_2 \quad (2\text{-}15)$$

It should be noted that M in reactions 2-13 and 2-14 is a third body, namely any other species in the gas phase that might collide with the excited complex (e.g. NO_2^* in 2-13) and remove the excess energy stabilising the molecule. In practice this is all stable molecular species as these make up the bulk of the gas mixture. The rate of such reactions therefore depends on the overall pressure of the system (Pilling and Smith 1987).

Nitric acid is produced in this reaction scheme by the following reactions:

$$OH + NO_2 + M \leftrightharpoons HNO_3 + M \quad (2\text{-}16)$$

$$N_2O_5 + H_2O \leftrightharpoons 2HNO_3 \quad (2\text{-}17)$$

The presence of argon in the system results in the following reactions:

$$Ar \xrightarrow{Rad} Ar^+ + e^- \quad (2\text{-}18)$$

$$Ar^+ + O_2 \rightarrow Ar + O_2^+ \quad (2\text{-}19)$$

$$Ar^+ + N_2 \rightarrow Ar + N_2^+ \quad (2\text{-}20)$$

$$Ar^+ + H_2O \rightarrow ArH^+ + OH \quad (2\text{-}21)$$

The impact of this chemistry is discussed in the following section.

For reducing conditions, excess H_2 present, ammonia can be formed in the system, the main mechanism being:

$$N + H_2 \leftrightharpoons NH + H \quad (2\text{-}22)$$

$$NH + H_2 \leftrightharpoons NH_2 + H \quad (2\text{-}23)$$

$$NH_2 + H + M \leftrightharpoons NH_3 + M \quad (2\text{-}24)$$

In total there are approximately 350 chemical reactions completing the reaction scheme used in the current model (see Appendix).

2.2 Equations for chemistry

The primary interactions are modelled with differential equations of the following type:

$$\frac{d[N]}{dt} = D_r G(N) \tag{2-25}$$

Where t is time, the brackets [] denote concentrations, $G(N)$ is the G-value[3] for nitrogen atom production from irradiation of N_2 and D_r is the dose rate to N_2 in the gas mixture (units 100 eV cm^{-3} s^{-1}). $\frac{d[N]}{dt}$ is therefore given in atoms cm^{-3} s^{-1}. The dose rate to N_2 is given by

$$D_r = D_r^T \frac{Z_{N_2}[N_2]}{Z_{N_2}[N_2]+Z_{O_2}[O_2]+Z_{H_2O}[H_2O]+Z_{Ar}[Ar]} \tag{2-26}$$

where D_r^T is the total dose rate to the system and Z_{N_2} etc are the number of electrons in the particular species, 14 for N_2 for example. The G-values used in the model are those originally utilised by Person and Ham (1988) and originate from the review by Willis and Boyd (1976). For gas phase systems G-values are largely independent of radiation type, more specifically LET (linear energy transfer rate) (see Spinks and Wood 1990), so the source of the dose rate is not too important.

The chemical reactions are modelled by solving the associated chemical rate equations, for example for reaction 2-5 it is possible to write:

$$\frac{d[O_2^+]}{dt} = -k[O_2^+][NO_2^-] \tag{2-27}$$

Here the rate of loss of O_2^+ due to this reaction is given by a second order rate equation with the rate constant k. It should be noted that:

$$\frac{d[O_2^+]}{dt} = \frac{d[NO_2^-]}{dt} = -\frac{d[O_2]}{dt} = -\frac{d[NO_2]}{dt} \tag{2-28}$$

as a consequence of this reaction and mass balance. For any particular species in the system many reactions may lead to its formation and destruction and so it is possible to write for any species, for example:

$$\frac{d[O_2^+]}{dt} = \sum_i R_i \tag{2-29}$$

where R_i is the rate of change of the species due to an individual reaction (e.g. Equation 2-27) and the summation is over all reactions that involve that species. Equations corresponding to 2-29 exist for all the species in the system and these must be integrated simultaneously with respect to time since any one species may impact on the rate of production/destruction of another.

Most of the ion-ion, ion-molecule reaction rate constants used here have little dependence on temperature, over the temperature range of interest, but many of the radical-radical, radical-molecule reactions do. As stated by Henshaw (1994) these constants often have an Arrhenius form:

$$k = AT^n \exp\left(-\frac{E}{T}\right) \tag{2-30}$$

where T is the temperature and the constants A, n and E have to be determined experimentally. For three body reactions the rate constants have the form:

$$k = \left[\frac{k_o k_\infty [M]}{k_o[M]+k_\infty}\right] F \tag{2-31}$$

where

$$\log(F) = \log(F_c) / \{1 + (\log\left(\frac{k_o[M]}{k_\infty}\right))^2\} \tag{2-32}$$

The rate constants for low (k_o) and high (k_∞) pressure are expressed in the Arrhenius form and F_c is an experimentally determined constant. Henshaw (1994) stated that the sources for the chemical rate constants were Tsang and Herron (1991), Baulch et al. (1974) and Warneck (1988).

[3] Number of atoms produced per 100 eV of radiation energy adsorbed.

In the current model these rate constants have been updated using the US National Institute of Standards (Manion et al. 2015) online data base of chemical rate constant data. Several additional reactions were also identified in this data base that had not been included in the Henshaw (1994) model and were added to the reaction set, e.g.

$$N + NH_3 \leftrightharpoons NH + NH_2 \tag{2-33}$$

$$k = 7.42 \times 10^{-12} \exp\left(-\frac{4830.4}{T}\right) \tag{2-34}$$

where the products *NH* and NH_2 have been assumed.

Most of the Henshaw (1994) ion-ion or ion-molecule rate constants originated from the paper by Person and Ham (1988) with some additional reactions and rate constants from Ikezoe et al. (1987). These rate constants have been updated for this work using the University of Manchester Institute of Technology astro-chemistry database (Woodall et al. 2007, also see UMIST web-site (2021)) and, where relevant, additional reactions from this database have been added to the model reaction set.

The most significant difference between the current model and that used by Henshaw (1994) is the inclusion of backward rates for each of the reactions utilising chemical thermodynamics. All the radical-radical, radical-molecule reactions are incorporated in both the forward and backward directions, for example for reaction (2-22)

$$N + H_2 \leftrightharpoons NH + H$$

The rate equations are now of the form:

$$\frac{d[N]}{dt} = k_b[NH][H] - k_f[N][H_2] \tag{2-35}$$

where k_f is the rate constant for the forward reaction and k_b the rate constant for the backward reaction. These rate constants are related by:

$$K_{eq} = \frac{k_f}{k_b} \tag{2-36}$$

where K_{eq} is the thermodynamic equilibrium constant for the reaction expressed in the appropriate concentration units. So, knowing the forward rate and equilibrium constant it is possible to calculate the backward rate. The equilibrium constant K_{eq} is given by:

$$K_{eq} = e^{\left(-\frac{\Delta G}{RT}\right)} \tag{2-37}$$

where R is the gas constant and the Gibbs free energy change, ΔG, is expressed in terms of the enthalpy and entropy changes for the reaction by:

$$\Delta G = \Delta H - T\Delta S \tag{2-38}$$

To calculate the enthalpy and entropy changes for each reaction it is necessary to know the enthalpy and entropy of each of the gas phase species. The enthalpy and entropy of each of the species is given by expressions of the following type

$$\frac{H}{RT} = a_0 + \frac{1}{2}a_1T + \frac{1}{3}a_2T^2 + \frac{1}{4}a_3T^3 + \frac{1}{5}a_4T^4 + \frac{a_5}{T} \tag{2-39}$$

$$\frac{S}{R} = b_0 \log(T) + b_1T + \frac{1}{2}b_2T^2 + \frac{1}{3}b_3T^3 + \frac{1}{4}b_4T^4 + b_5 \tag{2-40}$$

The constants a_0, a_1, … b_0, b_1… for each species were obtained from the CHEMKIN thermodynamics database (Kee et al. 2000][4].

[4] It should be noted that the thermodynamic standard state for gases is usually expressed in terms of gas pressures and the equilibrium constant therefore in terms of partial pressures. Chemical kinetics is usually expressed in concentration units (moles cm^{-3}, moles dm^{-3} etc), meaning Equation 2-36 usually has to be multiplied by $(RT)^n$ to effect a units conversion, were n depends on the order of the reaction.

2.3 Equations for evaporation and corrosion

2.3.1 Evaporation

If liquid water is present in the canister, then the concentration of water in the gas space will be maintained at the saturation vapour pressure for the local temperature. Since water is consumed either by corrosion or through radiolysis an equation has to be included to maintain the water equilibrium partial pressure. Therefore, the following equation for the gas phase water concentration was included in the model:

$$\frac{d[H_2O]_g}{dt} = k_e f - k_e[H_2O]_g \quad (2\text{-}41)$$

and

$$\frac{d[H_2O]_{liq}}{dt} = -\frac{d[H_2O]_g}{dt} \quad (2\text{-}42)$$

k_e is the evaporation rate constant, $[H_2O]_{liq}$ is the concentration of liquid in the system (moles of liquid water present divided by system volume) and $[H_2O]_g$ the gas phase concentration of water..

The function f is defined by

$$f = [H_2O]_{eq}\exp\left(-10^{-14}/(RAMP([H_2O]_{liq}) + 10^{-17})\right) \quad (2\text{-}43)$$

$[H_2O]_{eq}$ is the equilibrium concentration of gaseous water determined by the vapour pressure at the system temperature. The RAMP function is defined by:

$$RAMP(x) = \frac{x+|x|}{2} \quad (2\text{-}44)$$

where $|x|$ is the absolute value of the term inside the brackets. This definition means that when $[H_2O]_{liq}$ becomes small ($< 10^{-17}$ mole cm^{-3}) or negative, the term $RAMP([H_2O]) + 10^{-17} \sim 10^{-17}$, so that $f \sim 0$, but when $[H_2O]_{liq}$ is larger than 10^{-14} $f \sim [H_2O]_{eq}$. The function f behaves very much like a Boolean Switch function, being zero when there is little or no liquid water in the system and being equal to the vapour pressure of water when liquid is present. However, it is slightly less discontinuous than a switch function and enables a smoother integration of the equations. With this definition it is clear that when liquid water is present in the system Equation 2-41 becomes

$$\frac{d[H_2O]}{dt} = k_e[H_2O]_{eq} - k_e[H_2O]_g = k_e([H_2O]_{eq} - [H_2O]_g) \quad (2\text{-}45)$$

meaning if the gas phase concentration of water is less than the equilibrium vapour pressure it will increase at this rate, while Equation 2-42 means that the amount of liquid decreases at the same rate. This will continue until $[H_2O] = [H_2O]_{eq}$ at which point evaporation stops (rate goes to zero) and the gas phase concentration remains at the equilibrium vapour pressure. The evaporation rate k_e was chosen to be large so that equilibrium is established rapidly.

2.3.2 Equations for corrosion

There are two corrosion processes of the carbon steel inner liner that might occur within the canister, under aerobic conditions (oxygen present) the corrosion reaction is

$$4Fe + 2H_2O + 3O_2 = 4FeOOH \quad (2\text{-}46)$$

consuming both O_2 and H_2O. Constant corrosion rates of 0.2 or 0.4 mm/y were chosen for this reaction based on the work of Swanton et al. (2015), Sridhar et al. (1994), Speller (1951) and Uhlig et al. (1985). The value of 0.4 mm/y corresponds to 70 ºC and given that the duration of this corrosion mode is a few hours, higher temperatures and corrosion rates were not tested. Instead, a lower corrosion rate of 0.2 mm/y, typical for room temperature corrosion of carbon steel in oxygenated water was also tested.

For anaerobic (no oxygen) conditions the corrosion of the steel involved water and leads to H_2 production:

$$3Fe + 4H_2O = Fe_3O_4 + 4H_2 \quad (2\text{-}47)$$

A constant corrosion rate of 0.003 mm/y was assumed for this reaction based on the experimental work of Smart and Rance (2005), which measured the anoxic corrosion rate of cast iron at 30 ºC and in the presence of γ-radiation[5]. Given the higher temperature in the canister, this corrosion rate is assumed to be pessimistic.

The following differential equations were implemented in the model to simulate this corrosion behaviour:

Aerobic conditions:

$$\frac{d[O_2]}{dt} = -\frac{3}{4}C_1 f_1 f_2 \quad (2\text{-}48)$$

$$\frac{d[H_2O]}{dt} = -\frac{1}{2}C_1 f_2 f_1 \quad (2\text{-}49)$$

For anaerobic conditions

$$\frac{d[H_2O]}{dt} = -\frac{4}{3}C_2(1 - f_1)f_2 \quad (2\text{-}50)$$

and

$$\frac{d[H_2]}{dt} = -\frac{d[H_2O]}{dt} \quad (2\text{-}51)$$

Here C_1 and C_2 are the corrosion rates in the appropriate units, given by:

$$C_1(moles\ cm^{-3}s^{-1}) = \frac{C_{AE}A\rho_{Fe}}{V\times 1.77\times 10^9} \quad (2\text{-}52)$$

$$C_2(moles\ cm^{-3}s^{-1}) = \frac{C_{AN}A\rho_{Fe}}{V\times 1.77\times 10^9} \quad (2\text{-}53)$$

The factors ¾, ½, and 4/3 in Equations 2-48, 2-49 and 2-50 are a result of the stoichiometry of the two corrosion reactions. Here C_{AE} and C_{AN} are the aerobic and anaerobic corrosion rates in mm/y, A is the iron surface area (mm^2), ρ_{Fe} the density of Fe (g/mm^3) and V (cm^3) the free gas volume in the system. The factor 1.77×10^9 is the atomic weight of Fe multiplied by the number of seconds in a year. The functions f_1 and f_2 are similar to f in Equation 2-43 and fulfil a similar purpose:

$$f_1 = \exp\left(-10^{-8}/(RAMP([O_2]) + 10^{-10})\right) \quad (2\text{-}54)$$

$$f_2 = \exp\left(-10^{-8}/(RAMP([H_2O]) + 10^{-10})\right) \quad (2\text{-}55)$$

If [O_2] falls below 10^{-10} moles cm^{-3} then $f_1 \sim 0$, otherwise $f_1 \sim 1$ and likewise for f_2 in relation to [H_2O]. These amount to approximately 1 ppm in the gas phase of O_2 and H_2O and the consequences, from Equations 2-48, 2-49 and 2-50 mean that if O_2 falls below this level aerobic oxidation ceases, but anaerobic oxidation occurs unless H_2O also falls below this value in which case both aerobic and anaerobic oxidation cease. From the results shown below aerobic oxidation initially in the system may consume O_2, so that aerobic oxidation ceases but anaerobic oxidation continues provided water above 1 ppm is present. However, water radiolysis may later produce O_2 in the gas phase and if this occurs aerobic oxidation may start again, if this occurs then the above equations will take this into account and allow the integration to proceed smoothly.

All the above equations form a set of simultaneous ordinary differential equations in time that must be solved starting with an initial set of boundary conditions and to do this the numerical integration package FACSIMILE was used (Curtis and Sweetenham 1987). This uses a robust form of Gears method (Gear 1971) with variable time stepping to perform the integration, which is essential for this problem in which the primary radiation interactions are happening on a 10^{-4} s time scale, the gas chemistry is happening on a 10^{-3} s time scale, corrosion is occurring on the 10^7 s time scale and the behaviour of the whole system is of interest over a 10^{10} s time frame, corresponding to the half-life of some of the major radioactive isotopes present, e.g. Cs-137. Even with a robust numerical integration tool a number of convergence problems had to be overcome to obtain solutions to the equations for certain initial conditions.

[5] Dose rate of 11 and 300 Gy/h were used in these experiments.

3 Model validation calculations

For a model containing so many equations and associated input parameters it is important to verify it provides reasonable results before applying it to the KBS-3 canister system. In order to do this a series of calculations have been performed and compared with results from a number of laboratory studies. These experiments and the model comparisons are discussed here.

3.1 Comparisons with the experiments of May and Jones

In his initial analysis of nitric acid production in the KBS-3 canister Marsh (1990) used a G-value for nitric acid production of 2 (i.e., 2 molecules of HNO_3 are produced for every 100 eV of energy adsorbed). This G-value was based on the experimental work of Jones (1959) and May et al. (1976). These experiments used an electron beam to irradiate moist air mixtures in sealed ampoules at water vapour pressures in the range 0.25–2.5 mmHg. The ampoules contained liquid water to maintain a constant vapour pressure and the dose rate from the electron beam was large, 1.7×10^{20} eV $min^{-1}cm^{-3}$. After a particular dose the ampoules were broken in alkali containing water and the pH change of the water measured to obtain the acid content of the ampoule. In the model used here only the gas chemistry is simulated, but clearly in these experiments any acid produced within the ampoule would be captured by the liquid water present. In fact, any oxidised form of nitrogen within the ampoule is likely to be measured as acid once the ampoule is exposed to the alkaline solution. Therefore, to simulate these experiments, it has been assumed that HNO_3, HNO_2, NO_2, NO and N_2O is captured by the water during the irradiation. This will undoubtedly be the case for any acids produced, but is less obvious for the nitrogen oxides. However, it should be realised that the liquid water inside the ampoule is also been irradiated during the course of these experiments, producing aqueous OH, H_2O_2 etc so it is likely that species such as NO_2 dissolving in the water would be oxidised to HNO_3 (see Ibe et al. 1989). Modelling the chemistry in both phases along with gas partitioning is feasible, but at this stage the simple assumption mentioned above is made instead. The simulated amount of nitrous material captured by the water is reported as “acid” in the Figure 3-1.

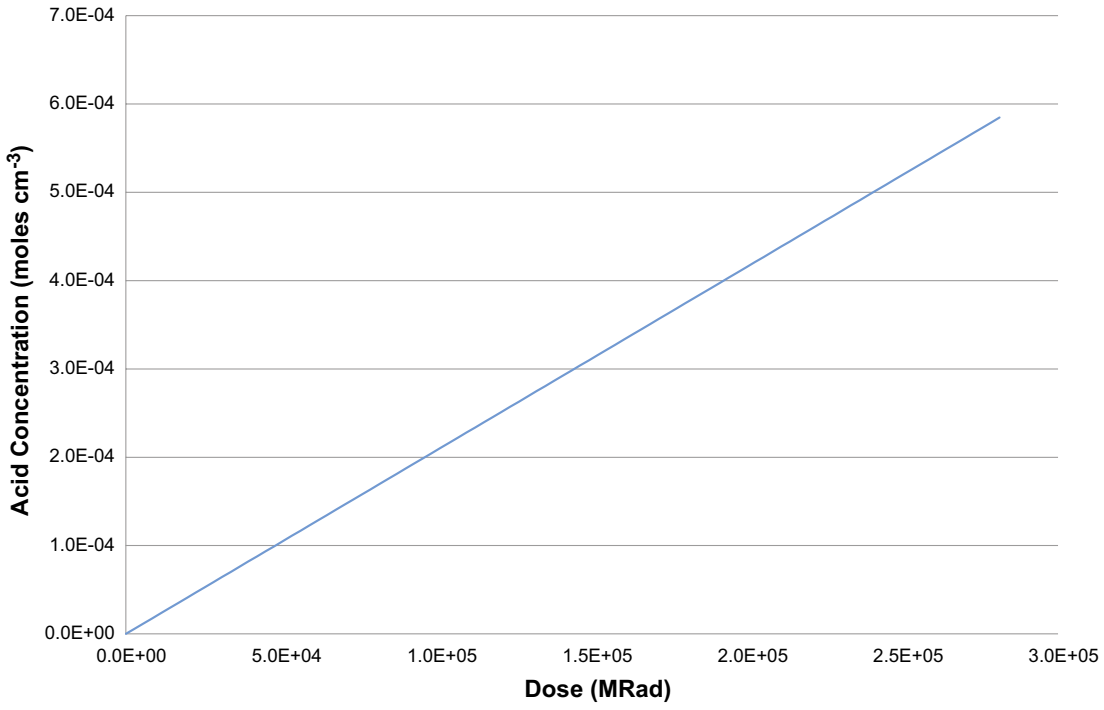

Figure 3-1. *Plot of modelled acid against dose simulating the experiments of May et al. (1976).*

The production rate of acid is constant for the dose plotted and corresponds to a simulated G-value for acid of 1.87, which is in reasonable agreement with the Jones experimental value of 2.

The irradiation of moist air mixtures in the presence of noble gases has been discussed in detail by Henshaw (1994), but is considered again here (a) for completeness and (b) to re-assess the Henshaw (1994) results with the new model developed for this work.

The $^{14}N_2$-$^{15}N_2$ isotope exchange studies of Wood and Mascall (1975) implied noble gases enhanced exchange. The work stated this was a result of enhanced N_2^+ formation from the charge transfer between radiolytically produced Ar^+ and N_2. Linacre and Marsh (1981) irradiated moist air mixtures combined with helium in a test reactor and concluded this lowered the G-value for acid production. The work of May et al. (1976) suggested Ar increased the production of nitric acid in irradiated moist air mixtures. This conclusion was largely based on Figure 3-2 below, taken from May et al. (1976).

Figure 3-2 shows the amount of nitrate produced after irradiating a sample to a dose of 19 Mrads. All samples contained a gas volume of 170 cm^3 at 300 K irradiated at a dose rate of 1.1 Mrads/h. The experiment containing Ar was carried out at 700 mmHg total pressure, varying the partial pressure of Ar. The experiments for moist air were carried out at 700 mmHg, but then the pressure was dropped to lower the amount of gaseous air in the system. May et al. (1976) assumed that in two experiments in which the same mass of air was present in the gas space then the same amount of nitrate should be produced if Ar had no effect on the chemistry. Figure 3-2 therefore suggests the presence of Ar leads to increased amounts of nitrate production, since the sample containing Ar produce more nitrate than the equivalent sample with the same mass of air. However, what this assumption failed to recognise, and was pointed out by Henshaw (1994), is that several important rate constants leading to nitric acid production are pressure dependent, in particular the reaction (2-16) above. The experiments in the absence of Ar for equivalent gaseous air mass were performed at lower pressures than the experiments with Ar and this would probably lower the nitric acid production rate.

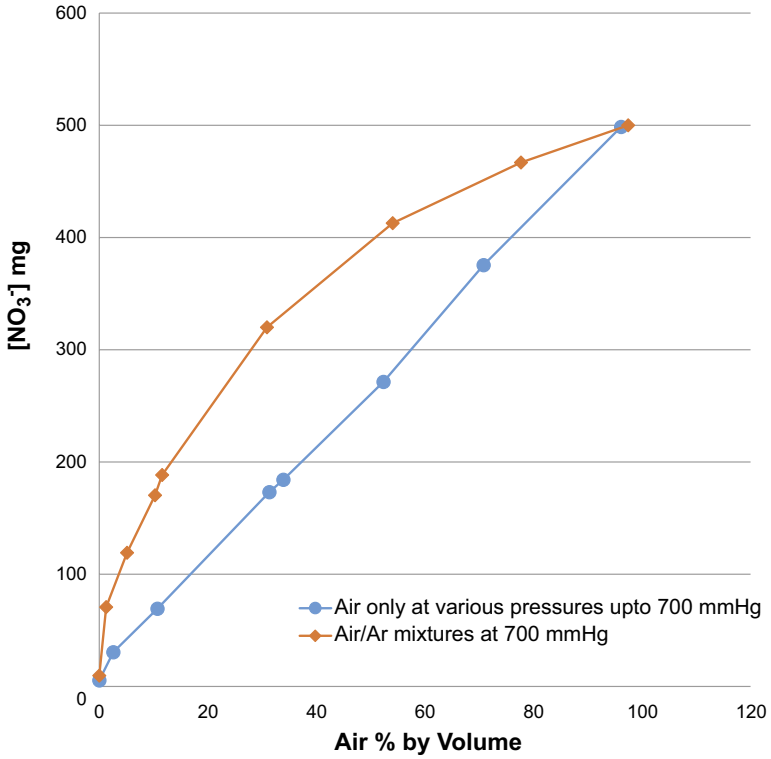

Figure 3-2. *Nitrate production as a function of % air for (a) moist air only and (b) moist air-Ar mixtures. Experimental results of May et al. (1976).*

Calculations have been performed with the new model for the experimental conditions of May et al. (1976) outlined above and the amount of nitric acid produced after a dose of 19 Mrads is plotted in Figure 3-3 against the fraction of air in an air/Ar mixture. Also plotted is the amount of nitric acid produced from the irradiation of an equivalent amount of moist air (assuming a constant water vapour pressure at 300 K).

The absolute amounts in Figures 3-2 and 3-3 should not be compared as the model does not simulate the liquid phase present in these experiments. However, the general behaviour displayed by the new model is similar to that observed in the experiments, in that more nitrate is produced in the Ar/moist air mixture than the irradiated equivalent masses of air. In order to test to what extent this difference is due to the different pressures of the two experiments and to what extent it depends on the chemistry introduced by the presence of Ar, a calculation was performed in which this chemistry was "switched off". In the model this is accomplished by not allowing the primary interactions of Ar with the radiation leading to Ar^+ or Ar^*. Removing the Ar chemistry, but still allowing it to act as a third body in the many three body reactions, i.e. keeping the pressure dependence, still leads to increased nitrate production, but not as much as when the Ar chemistry is present. The model suggests the apparent enhancement in nitrate production in these experiments is partly due to the pressure differences in the experiments and partly due to the new chemistry introduced from the presence of Ar. This conclusion is different than the one proposed by Henshaw (1994) who assigned the difference completely to the pressure differences. The current model contains a much greater number of reactions, as explained above and should represent the chemistry more accurately. With extensive investigation it would be possible to identify exactly what differences in the 1994 chemistry and the current model has resulted in these different conclusions, but for the purposes of the present study such an investigation is unnecessary. The model generally reproduces the impact of Ar and predicts acid concentrations compatible with experimental data.

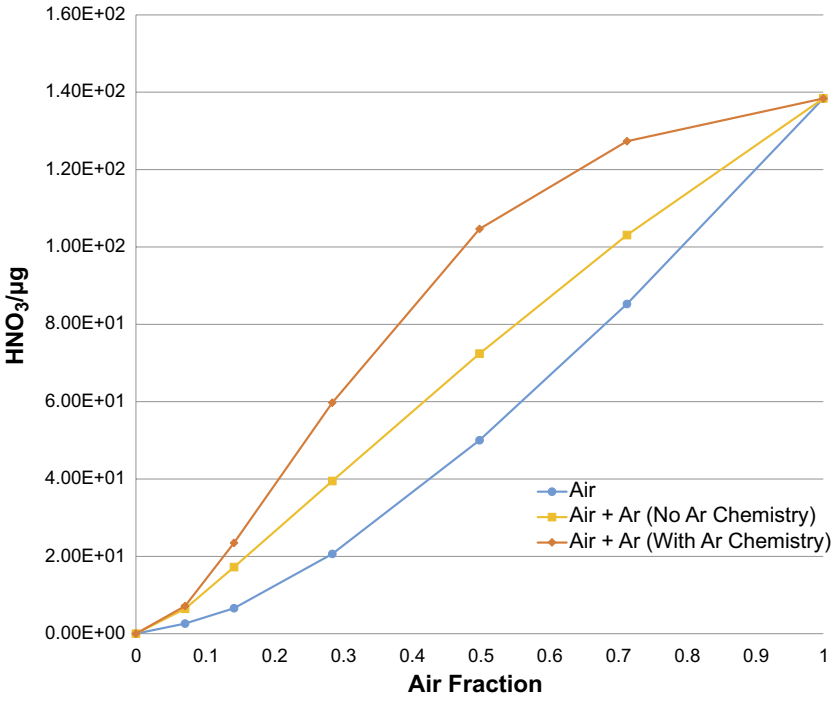

Figure 3-3. *Modelled nitrate production as a function of fraction of air for (a) moist air only and (b) moist air-Ar mixtures.*

3.2 Comparisons with the experiments of Tokunaga and Suzuki

In these experiments N_2 with added amounts of NO, NO_2, O_2 were irradiated using an electron accelerator in both a flow through system and using glass ampoules of mixed gasses. The dose rates for the two types of experiments were 0.29 and 0.14 MRads/s respectively and the gas composition (N-oxides) was measured as a function of time using chemiluminescence. The details of the experiments are discussed in Tokunaga and Suzuki (1984).

Figure 3-4 is a comparison of the model with an experiment of Tokunaga and Suzuki (1984) involving irradiation of N_2 containing an initial 250 ppm of NO.

The model reproduces well the destruction of NO, the initial formation of NO_2 and then its subsequent destruction to N_2 and O_2. Most importantly it captures the time scales of these processes relatively well.

Figure 3-5 shows a more interesting set of results in terms of relevant chemistry. In this experiment a mixture of NO, O_2, H_2O and N_2 was irradiated and the amounts of NO_2 and HNO_3 in the gas phase monitored as a function of time.

The results of Figure 3-5 are encouraging in that these experiments involve the irradiation of a gas phase mixture of O_2, N_2 and H_2O (no liquid phase present) and the model gives reasonable agreement with the experimental data, both in terms of the amount of nitric acid produced and the timescale for its production.

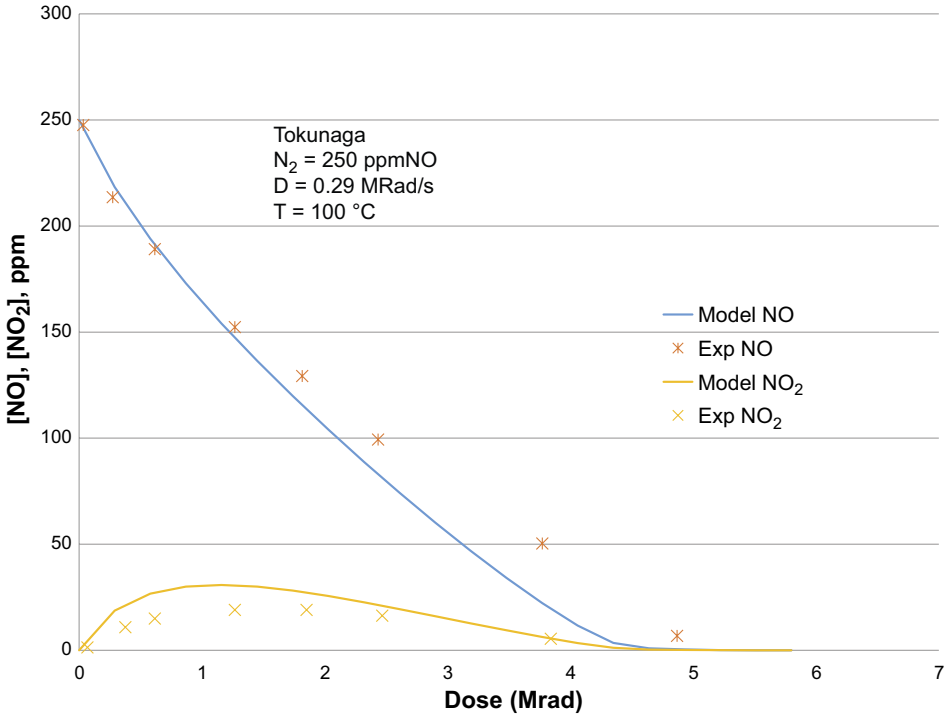

Figure 3-4. *Comparison of model results with Tokunaga experimental data. N_2 with 250 ppm NO.*

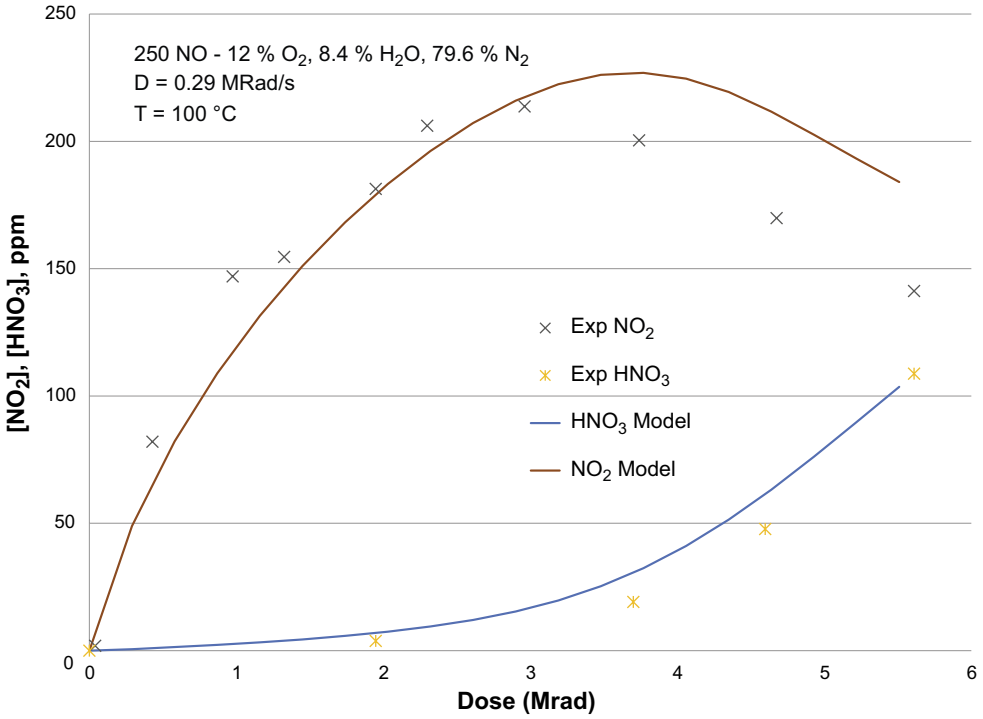

Figure 3-5. *Comparison of model results with Tokunaga experimental data. N_2 with 250 ppm NO, 12 % O_2 and 8.4 % H_2O.*

3.3 Comparisons with the experiments of Cheek and Linnenbom (1958)

The gas atmosphere inside the KBS-3 canister may become reducing in time as oxygen is consumed by corrosion and under these circumstances reduced forms of nitrogen may be produced, such as ammonia. Ammonia can potentially lead to altered corrosion mechanisms of the canister materials and so it is important to understand under what circumstances ammonia might form and if it forms then how much. The model therefore as well as simulating the formation of nitric acid also has to be able to simulate ammonia production. To validate this aspect of the model comparisons were made with the experimental results of Cheek and Linnenbom (1958). In these tests at high pressures (up to 100 atm.) various mixtures of N_2-H_2 were irradiated at 25 ºC with a Co-60 radiation source and the amount of ammonia measured by bubbling the resulting gases through water and measuring NH_3 spectrophotometrically after treating with a Nessler reagent. Figure 3-6 is a comparison of the model with the experimental data of Cheek and Linnenbom (1958) for an irradiated N_2/H_2 mixture. Experimentally the G-value for NH_3 production was reported by Cheek as 0.7–1.0, Figure 3-6 indicates the model over predicts the rate of NH_3 production, with a calculated G-value of 1.5.

Figure 3-7 is a comparison of the model with results of Cheek and Linnenbom (1958) for a mixture of N_2/H_2 containing a small amount of O_2.

Initially, for the first 50 h of the experiment, no ammonia is produced. During this period the presence of O_2 suppresses ammonia formation because of the more favoured route for N radicals leading to nitrogen oxide formation. Once O_2 has been consumed, ammonia production commences. The model reproduces the behaviour reasonably well, but again overestimates the rate of production of ammonia once it begins. On the whole the model provides a reasonable description of ammonia formation under reducing conditions, it generally over predicts the rate of production but from the perspective of the KBS-3 canister the model should therefore be conservative.

Having validated the model against a range of published experimental data, its application to the KBS-3 canister will be discussed below. All of the experiments discussed above are at much higher dose rates than are likely to be present in the KBS-3 canister and although dose rate effects on overall long term yields have been noted in the irradiation chemistry of gases (see Spinks and Wood 1990),

this is due to changes in the kinetics following primary production. That is, increases or decreases, in the rates of production of primary species lead to changes in subsequent chemistry that result in increases/decreases in long time yields. Often a (Dose Rate)$^{1/2}$ dependence is noted for long time yields. Since the current model accounts for both primary yields and all the subsequent chemical kinetics it will capture such dose rate effects.

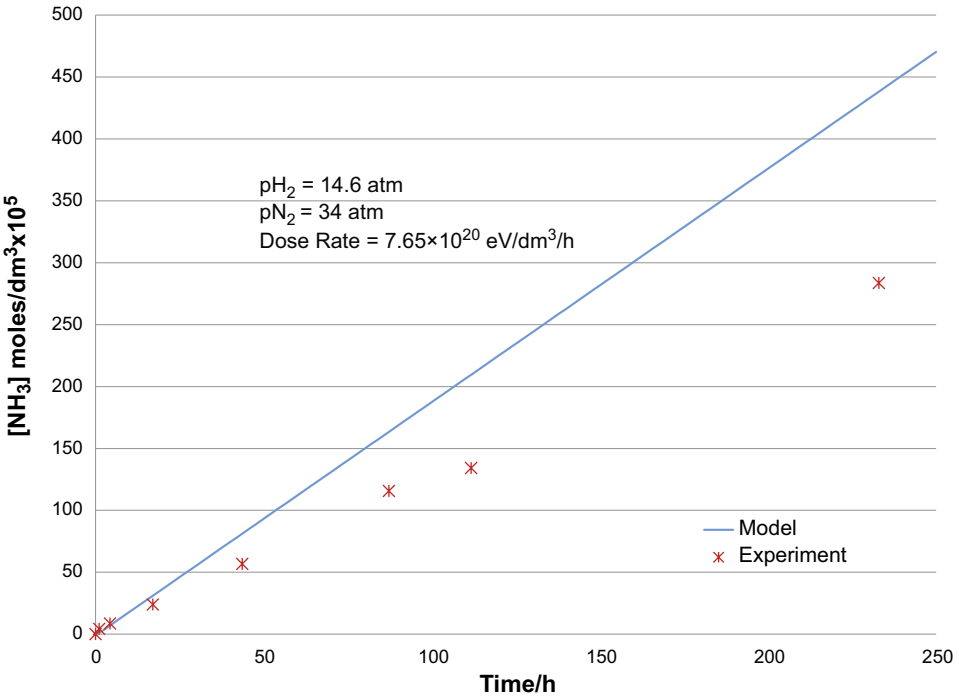

Figure 3-6. *Comparison of model results with Cheek and Linnenbom experimental data. N_2/H_2 gas mixture at 25 ºC.*

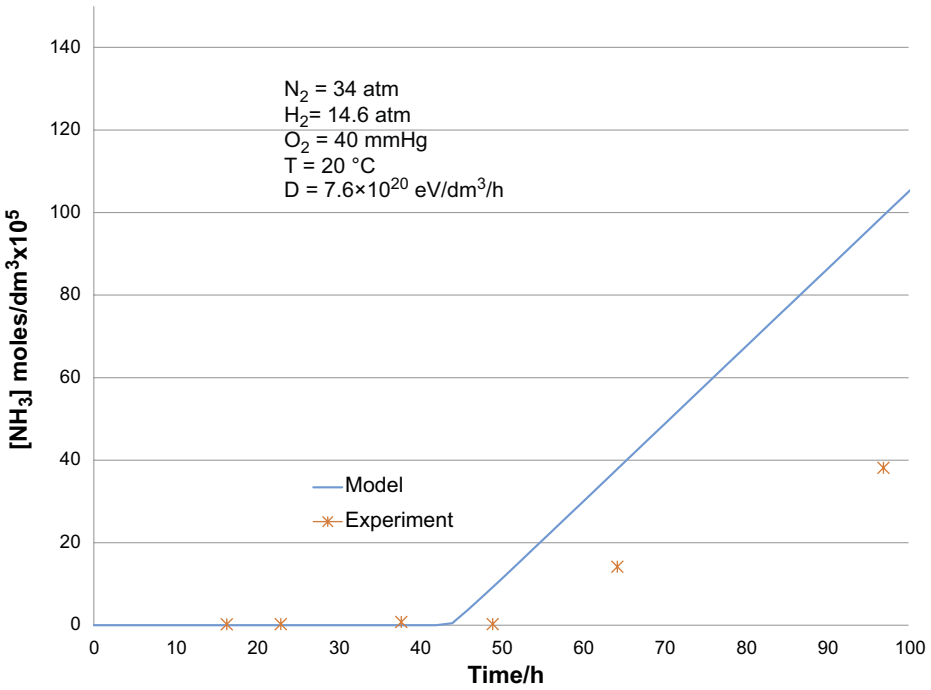

Figure 3-7. *Comparison of model results with Cheek and Linnenbom experimental data. N_2/H_2 gas mixture at 20 ºC, containing 40 mmHg of O_2.*

4 Application of the new N_2-O_2-H_2O-Ar radiolysis model to the KBS-3 canister

4.1 Definition of initial canister conditions – calculation cases/scenarios

In order to simulate the behaviour in the canister the following information is required:

- Gas temperature;
- Initial gas pressure and composition;
- Dose rate to the gas phase;
- Initial water content of the canister;
- Gas volume and available area for corrosion.

Many of the chemical rate constants used in the model are temperature dependent and so it is important to know how the KBS-3 canister temperature will evolve during its lifetime. A thermal analysis of the canister and surrounding landscape has been performed and the evolution of a BWR fuel filled canister temperature was reported by SKB (2006) and Figure 4-1 is taken from this reference.

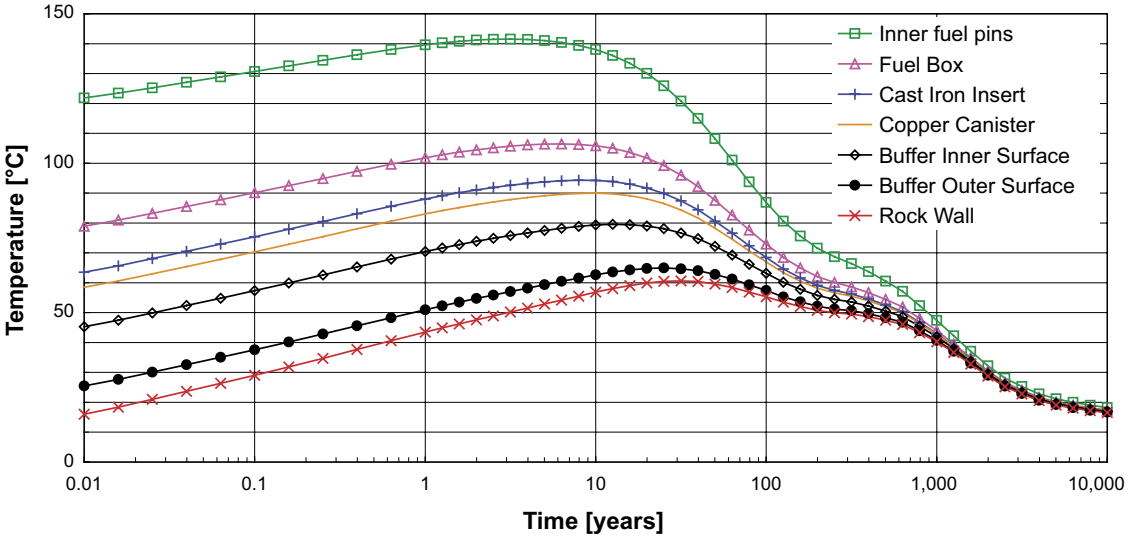

Figure 4-1. *Temperature – time evolution of various components of the KBS-3 canister, taken from SKB (2006).*

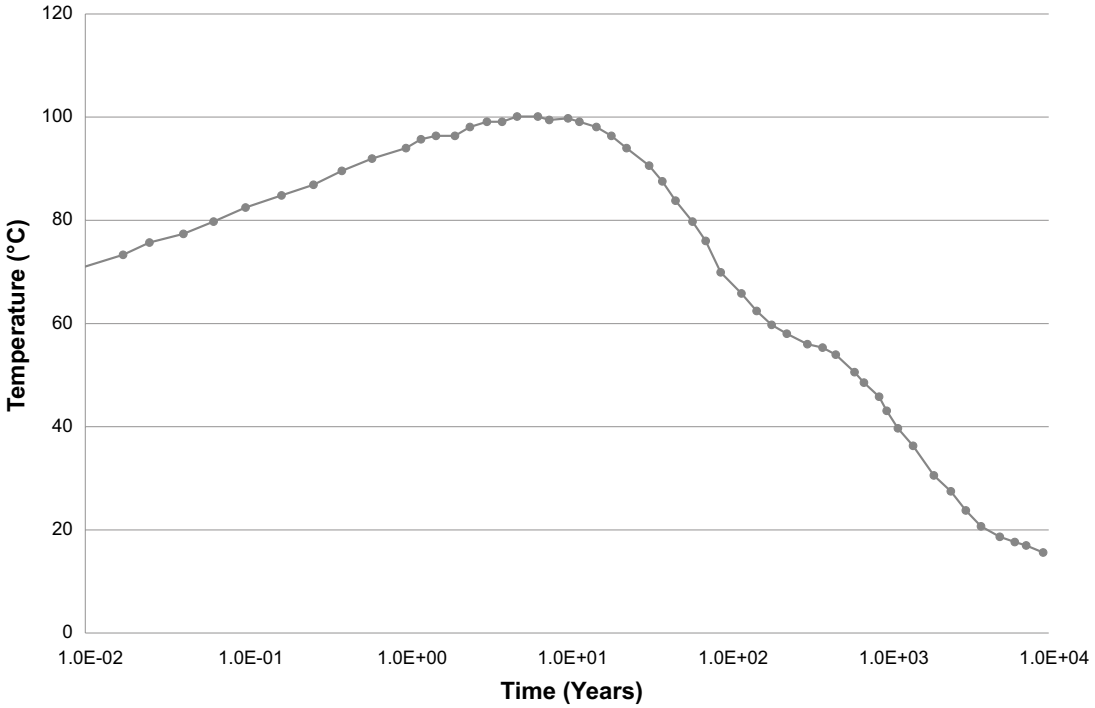

Figure 4-2. *Temperature – time evolution used in the model.*

For all the KBS-3 calculations discussed here, the temperature profile shown in Figure 4-2 was used.

This is an average of the fuel box and insert temperatures and was implemented explicitly in the model. This was done by including an array of temperature-time points in the code which was then utilised to calculate the system temperature at any integration time point by interpolation between the two closest times. Figure 4-2 is in fact temperature outputs from the model obtained by this process. At each time step during the numerical integration the temperature of the system is calculated internally by the model and all temperature dependent terms i.e. rate constants and thermodynamic terms, are continuously updated.

The canister is assumed to be initially at 1 atm pressure, however, if liquid water is present then as the system temperature rises so will the internal pressure, partly as a consequence of the increase in vapour pressure of the water. This evaporation is modelled, as described in Section 2 and the resulting system pressure updated throughout the calculation. As stated, several of the rate constants for the three body reactions depend upon the system pressure so it is important this is captured in the model. With regard to implementation in the model, an array of water vapour pressures over a range of temperatures was added to the computer code. The equilibrium water vapour pressure at any time during the integration was then calculated by first calculating the system temperature and then calculating the water vapour pressure by interpolation between the closest temperature points in the input temperature array.

The dose rates used in the model were the same as those used by Henshaw (1994), namely:

$$D = D_o \exp(-kt) \tag{4-1}$$

Where D_O is the initial canister dose rate of 310 Gy/h and the decay constant k is 7.3×10^{-10} s^{-1}, giving a dose rate half-life of approximately 30.1 years[6]. Clearly the dose rate depends on the amount and history of the stored fuel and so may vary from canister to canister. The initial dose rate used here is consistent with those reported by Willingham (1981) for BWR and PWR assemblies following 1–5 years pond storage after a burnup of 33 000 MWd/MT, but is high compared to the radiolysis analysis performed by Wittman (2013) for a US fuel storage canister design.

[6] The dose rate half life up to 500 y is primarily controlled by Cs-137 after which it decays less rapidly, most of the calculations present here are up to 500 y.

A free gas volume of 1 m^3 and surface area of 35 m^2 for the internal steel was used in calculating the gas consumption and production rates from corrosion (SKB 2010). These values are consistent (gas volume used here is slightly larger) with those reported by Neretnieks and Johansson (2014). The corrosion rates used for the calculations were given in Section 2.3.2 and it is assumed these are constant during the operational lifetime of the canister. Experiments suggest (Smart and Rance 2005) they are constant under moist air condition for more than a year, during which the greatest impact of corrosion on the gas chemistry is experienced in the model, so such an assumption seems reasonable.

Calculations were performed for a range of initial KBS-3 canister water masses and gas compositions. The maximum water content studied here was 600 g, which corresponds to 12 damaged fuel rods within the canister containing 50 g of water each (Neretnieks and Johansson 2014). The smallest water content considered here is 6.7 g of water corresponding to the residual water in a canister with one damaged and dried fuel rod[7]. The main gas component is Ar with small amounts of air. For the calculations performed here gas mixtures containing initially 10 % and 1 % air have been considered.

Table 4-1 lists all the cases/scenarios that have been modelled for the current study:

Table 4-1. Initial KBS-3 Conditions for Model Simulations*.

Cases$	Water (g)	Aerobic corrosion rate of steel mm/y (O_2 present)	Anaerobic corrosion rate of steel mm/y (No O_2 just water present)	O_2 (atm)	N_2 (atm)	Ar (atm)
1	600	0	0	0.021	0.078	0.901
2	600	0.4	3×10^{-3}	0.021	0.078	0.901
3	600	0.2	3×10^{-3}	0,021	0.078	0.901
4	6.7	0	0	0.021	0.078	0.901
5	6.7	0.4	3×10^{-3}	0.021	0.078	0.901
6	6.7	0.2	3×10^{-3}	0.021	0.078	0.901
7	244	0	0	0.021	0.078	0.901
8	244	0.4	3×10^{-3}	0.021	0.078	0.901
9	244	0.2	3×10^{-3}	0.021	0.078	0.901
10	600	0	0	0.0021	0.0078	0.9901
11	600	0.4	3×10^{-3}	0.0021	0.0078	0.9901
12	244	0	0	0.0021	0.0078	0.9901
13	244	0.4	3×10^{-3}	0.0021	0.0078	0.9901
14	6.7	0	0	0.0021	0.0078	0.9901
15	6.7	0.4	3×10^{-3}	0.0021	0.0078	0.9901

* Temperature profile given in Figure 4-2 used and dose rate given by Equation 4-1.

$ 1 = high H_2O, air, no corrosion, 2 = high H_2O, air, corrosion, 3 = high H_2O, air, low corrosion, 4 = low H_2O, high air, no corrosion, 5 = low H_2O, high air, corrosion, 6 = low H_2O, high air, low corrosion, 7 = intermediate H_2O, high air, no corrosion, 8 = intermediate H_2O, high air, corrosion, 9 = intermediate H_2O, high air, low corrosion, 10 = high H_2O, low air, no corrosion, 11 = high H_2O, low air, corrosion, 12 = intermediate H_2O, low air, no corrosion, 13 = intermediate H_2O, low air, corrosion, 14 = low H_2O, low air, no corrosion, 15 = low H_2O, low air, corrosion.

It is thought that calculations for all the initial conditions outlined in Table 4-1 should provide a reasonably clear picture of radiolysis behaviour within the KBS-3 canister.

[7] Spahiu K, 2020. Residual water in a KBS-3 canister and its effect on post-closure safety. SKBdoc 1914189 ver 1.0, Svensk Kärnbränslehantering AB. (Internal document.)

4.2 KBS-3 canister model results

4.2.1 Case 1 – high water content and no steel corrosion

Case 1 simulates the situation in which the water content of the canister is relatively high (12 failed fuel rods), there is significant (10 %) air trapped during backfill with Ar and no corrosion is occurring on the iron surface.

Figure 4-3 shows the canister temperature, pressure and dose rate output by the model for the first 500 years of storage.

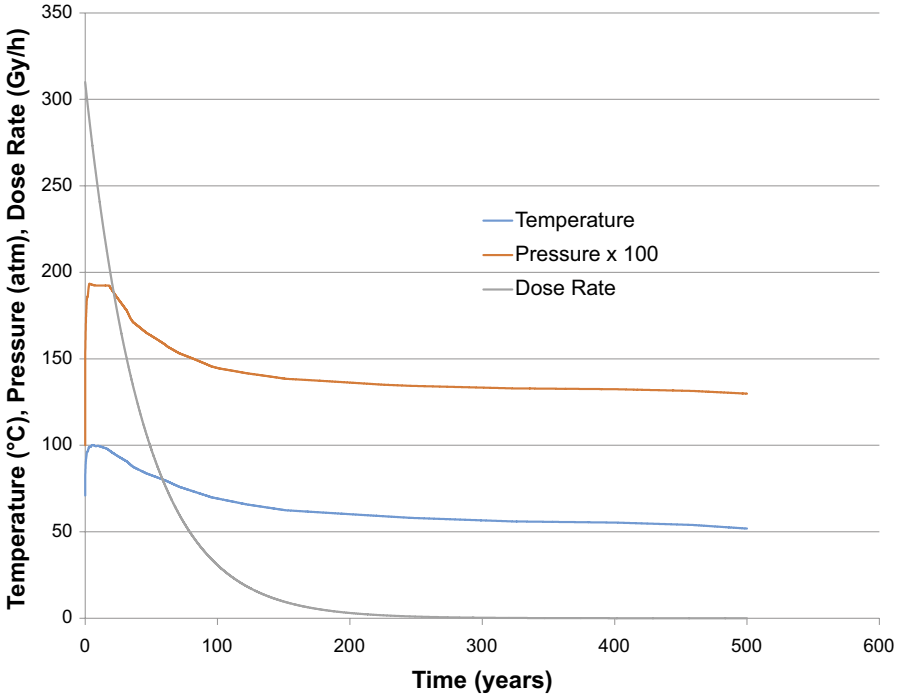

Figure 4-3. *Model calculated temperature, pressure and dose rate.*

The initial increase in canister pressure is a consequence of the temperature rise and vaporisation of the liquid water present, as shown in Figure 4-4.

The rise in water vapour pressure as the temperature increases just above 100 °C is matched by a loss in the liquid phase. After 500 years approximately 100 g of water has been converted into other species in the system as a consequence of the radiolysis. Of course, when iron corrosion is occurring all water is consumed in less than 2 years[8]. The real system will undoubtedly be more complicated with hot and cold regions within the canister where evaporation and condensation are occurring, but such spatial variations are not captured in this model. Figure 4-5 shows the calculated species concentrations for Case 1.

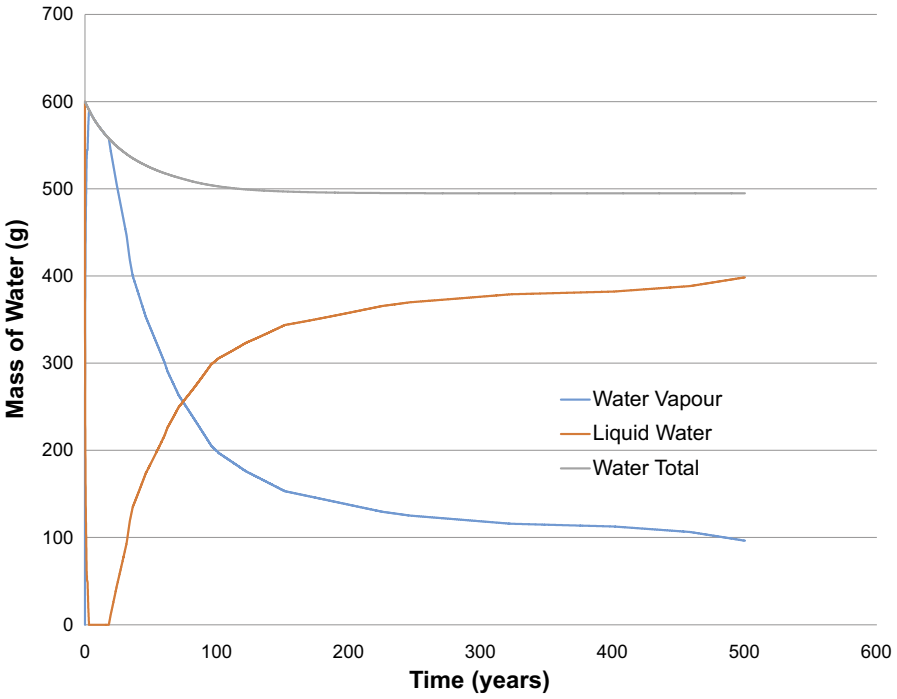

Figure 4-4. *Calculated amounts of water vapour, liquid water and total amount of water in the system versus time.*

[8] Spahiu K, 2020. Residual water in a KBS-3 canister and its effect on post-closure safety. SKBdoc 1914189 ver 1.0, Svensk Kärnbränslehantering AB. (Internal document.)

Figure 4-5 shows that after approximately 500 years of operation the system reaches a steady state with approximately 0.8 moles of nitric acid present, along with 2 moles of H_2O_2 and 3 moles of H_2. All the original O_2 in the system (0.7 moles) has been converted to other species and virtually no NH_3 has been produced. There is an initial period of 10^3 h (roughly 40–50 days) when little nitric acid is produced, this is consistent with the experimental results of Tokunaga and Suzuki (1984), see Figure 3-5. An initial incubation period occurs in the production of the acid as NO_2, the precursor to HNO_3 is formed. The experiments of Tokunaga and Suzuki (1984) are at higher dose rates than in the canister, so this period is much shorter in the experimental studies. It should also be noted that other species are present, e.g. HNO_2, NO_2, NO etc, which have not been plotted because individually they contribute only a small fraction to the gas phase mass, but collectively make a significant contribution. The model outputs the number of N, O and H moles in the system contained in all species present, which should be a constant throughout the calculation, which it is to the 10th significant figure. It should also be noted that around 10^6 hours there is a small "kink" in the nitric acid plot. Such discontinuities (which are also noted in later plots) are not due to any physical phenomena in the system but are a consequence of the models numeric's. For the current calculations an integration accuracy of 10^{-3} (3 significant figures) was adequate to obtain a solution up to the discontinuity point, but then ran into convergence problems and the integration accuracy had to be increased. Performing the whole calculation with a small integration accuracy is possible but would then take a very long time to complete, with very little gain in useful information. It should also be noted that it takes approximately 100 years for the species concentrations to reach steady state, which is approximately a factor of 5 longer than the calculations performed by Henshaw (1994) for the ACPC design. This earlier work did not include the reverse chemical rate processes, as discussed above, which will slow the rate of formation of HNO_3, NH_3 etc down.

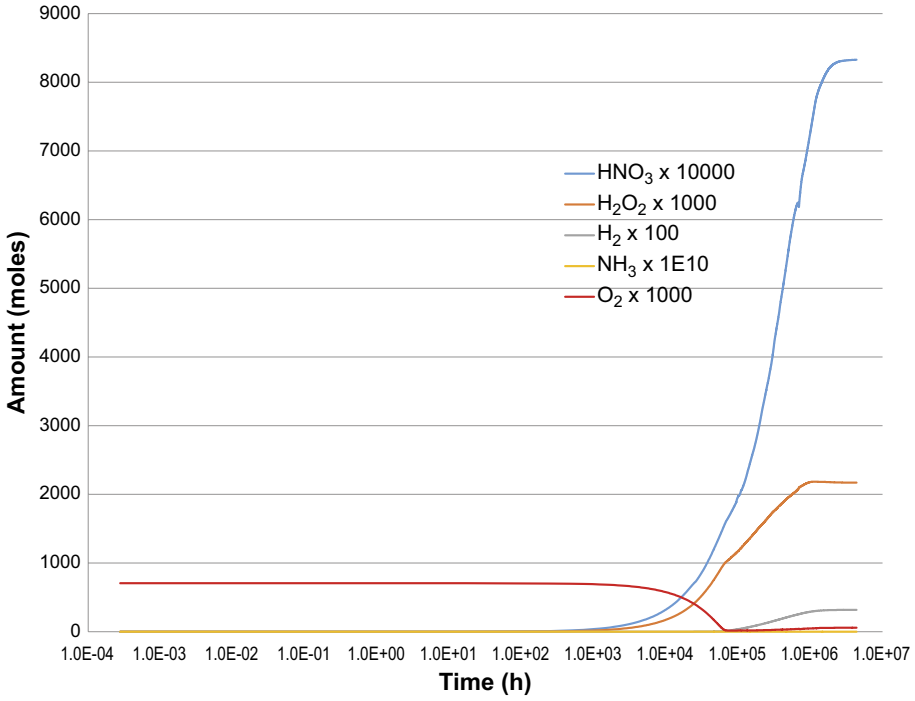

Figure 4-5. *Species concentrations versus time for Case 1, high water content, no corrosion.*

4.2.2 Case 2 – high water content with steel corrosion

Case 2 simulates the situation in which the water content of the canister is relatively high (12 failed fuel rods), there is significant (10 %) air trapped during backfill with Ar and corrosion is occurring on the carbon steel and cast-iron surface.

Figure 4-6 is a plot of the calculated water content (vapour + liquid), oxygen content and aerobic and anaerobic corrosion rates in the model. The corrosion rates are the C_1 and C_2 terms multiplied by the appropriate *f* terms, see Section 2. From the figure it is clear O_2 disappears quite rapidly from the system (< 10 h) due to corrosion and water is subsequently lost after approximately 10^4–10^5 h (~1,6 y). Once O_2 is lost aerobic oxidation ceases and anaerobic corrosion begins, and this stops when all the water in the system has been consumed.

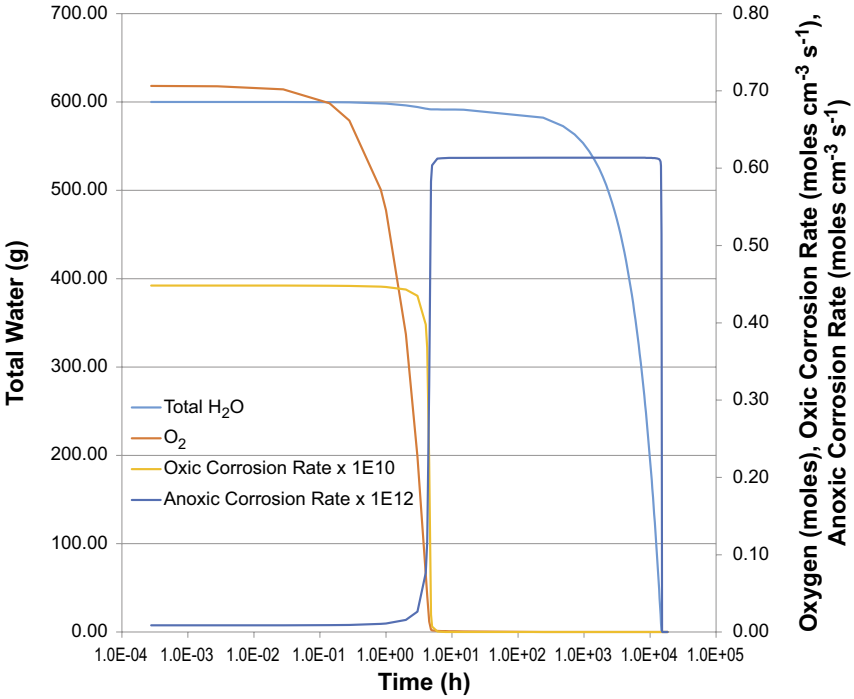

Figure 4-6. *Model outputs of canister water, oxygen, and corrosion rates versus time for Case 2.*

Figure 4-7 shows the predicted behaviour of the major species in the canister.

Nitric acid is produced during the first 10 h of operation while O_2 is present in the system, but then starts to decrease as both O_2 and H_2O_2 are lost. O_2 is lost via corrosion but H_2O_2 is lost as H_2 starts to be produced from anaerobic corrosion. The gas phase radiolysis reactions will reform H_2O from H_2O_2 and H_2 which is subsequently lost via anaerobic oxidation. With the loss of O_2 and H_2O from the system NH_3 starts to form until a steady state concentration of H_2 and NH_3 are achieved. This mixture also contains small amounts of nitric acid, which in reality would probably precipitate out as NH_4NO_3 but this process is not simulated in the model. It should be noted that liquid water exists for a short period of time while ammonia is forming.

The amount of nitric acid produced in the system for Case 2 is very small (of the order of 10^{-5} moles) compared to Case 1 in which no corrosion was included in the model (of the order of 1 mole). For Case 1 nitric acid production doesn't become significant until > 100 h of operation but for Case 2 O_2 has been removed well before this, by 10 h, and H_2 production from water corrosion has started suppressing other oxidants in the system, in particular H_2O_2 and OH. Since the primary mechanism for HNO_3 formation is OH + NO_2 + M = HNO_3 + M, nitric acid formation is suppressed before any significant build up. The ability of H_2 to suppress oxidant formation is well recognised in the liquid state (see Bartels et al. 2013) and is the reason it is added to water cooled nuclear reactor systems.

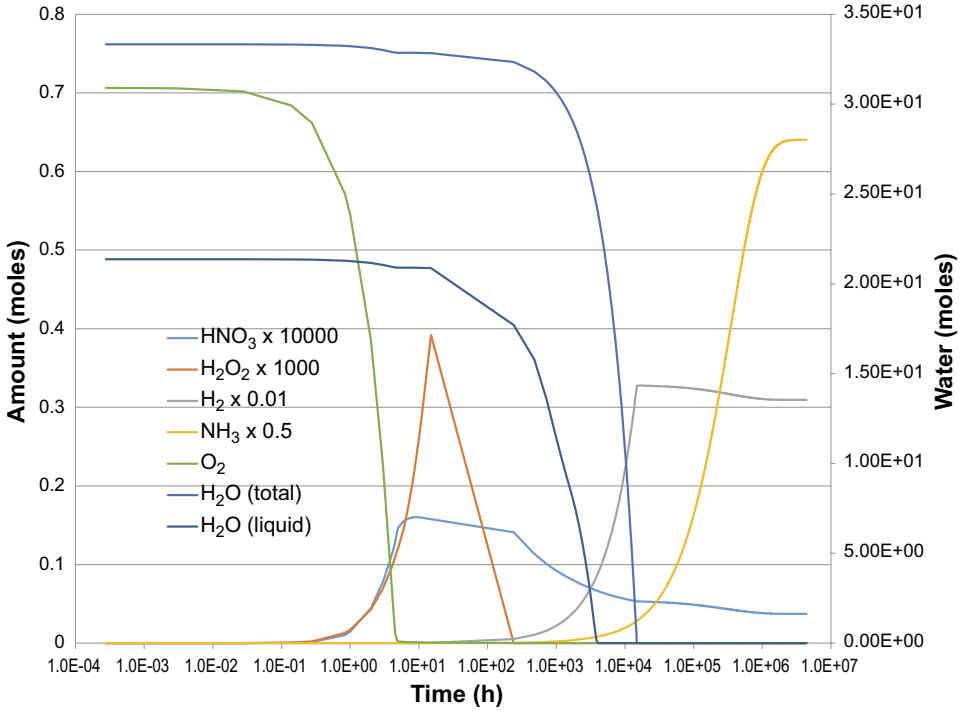

Figure 4-7. Calculated major species concentrations for Case 2, 600 g H_2O, 10 % air and corrosion.

4.2.3 Case 3 – high water content with steel corrosion (lower corrosion rate)

Case 3 is similar to Case 2 but with a lower aerobic corrosion rate. Figure 4-8 shows the behaviour of O_2, H_2O along with the corrosion rates for this scenario.

Figure 4-8 shows the lower aerobic corrosion rate which increases the time required to remove O_2 and subsequently lead to anaerobic oxidation and finally water removal from the system. On the time scales of the canister operational period these impacts are small though, as shown in Figure 4-9 which plots the calculated main species concentrations against time.

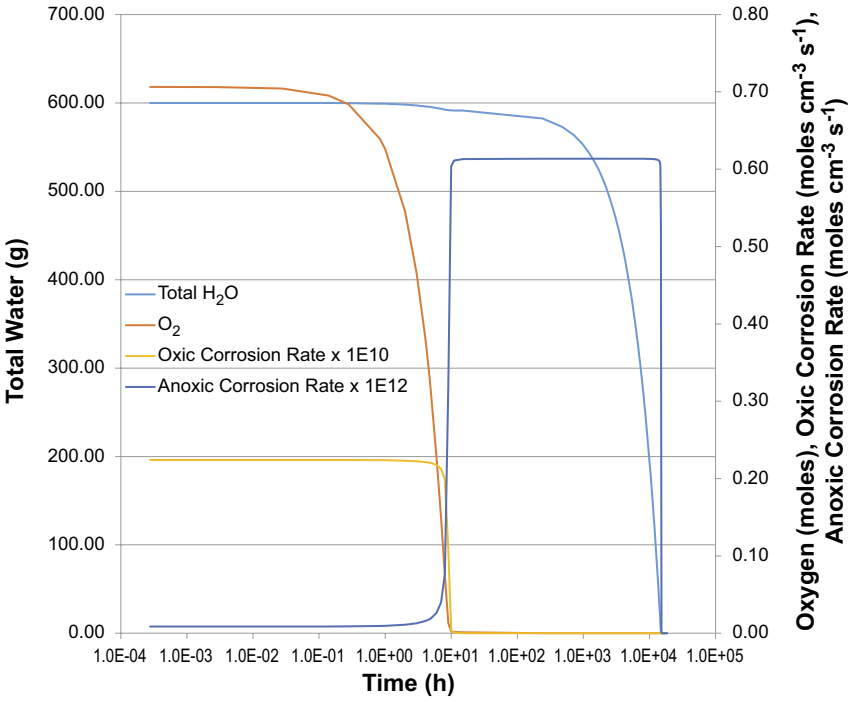

Figure 4-8. *Model outputs of canister water, oxygen, and corrosion rates versus time for Case 3.*

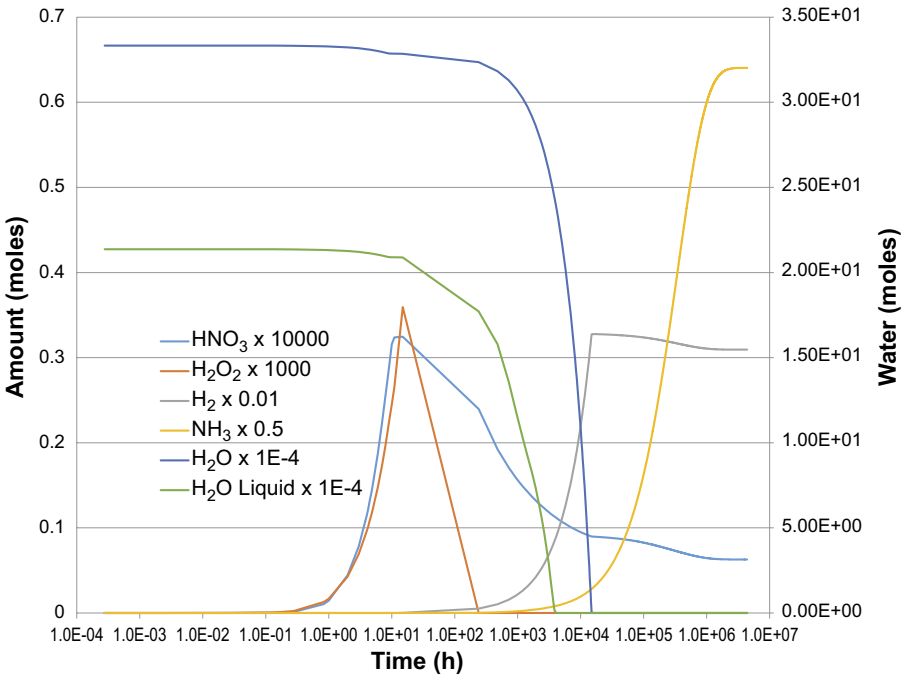

Figure 4-9. *Calculated major species concentrations for Case 3, 600 g H_2O, 10 % air and low corrosion rate.*

The general behaviour of the system is very similar to Case 2, the lower aerobic corrosion rate leads to more HNO_3 produced, although the absolute amount is still small (see Figure 4-10). The change in corrosion rate has virtually no effect on the formation of NH_3 (see Figure 4-11). The higher nitric acid concentration is simply a consequence of the slower removal of oxidant by corrosion.

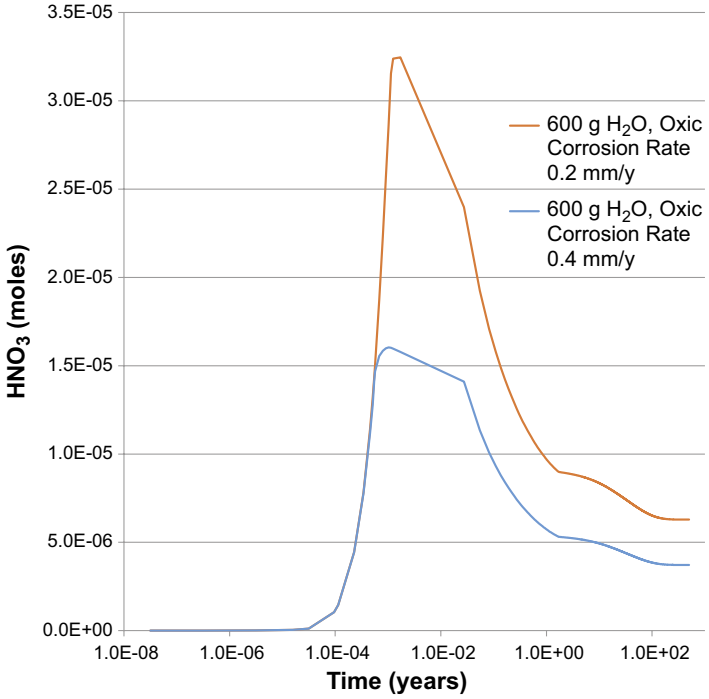

Figure 4-10. *Calculated nitric acid amounts for Cases 2 and 3, same initial conditions except for aerobic oxidation rates.*

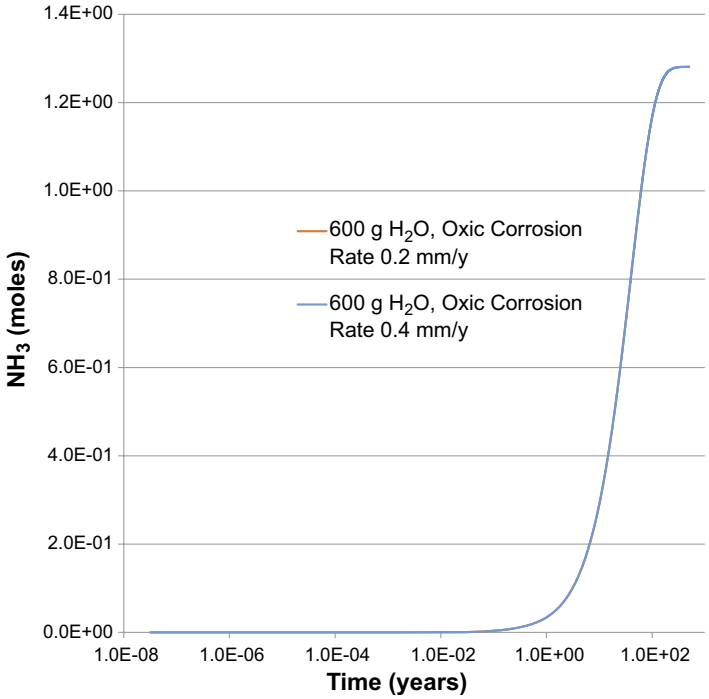

Figure 4-11. *Calculated ammonia amounts for Cases 2 and 3, same initial conditions except for aerobic oxidation rates. Cases overlap on the Figure.*

It should be noted from Figures 4-7 and 4-9 there is a short period of approximately 150 days between 10^3 and 10^4 hours of canister operation when both ammonia and water exist in the system for these high water cases.

4.2.4 Case 4 – low water content with no steel corrosion

For this simulation the 6.7 g of water was initially included in the model as liquid, but at the initial canister temperature and free gas volume this is rapidly all converted to water in the vapour state. Figure 4-12 shows the behaviour of the main species over the 500 y period that the canister is modelled.

Figure 4-12 shows quite a complex species behaviour over the 500 y modelled operational period of the canister. From 0.1–1 years both H_2O_2 and HNO_3 start to form with loss of O_2 and H_2O from the system, with a small amount of H_2 also produced from the radiolysis. All three species HNO_3, H_2O_2 and H_2 continue to increase up to around 10 years of operation at which point there is a fall in the amounts of H_2 and H_2O_2. There is a decrease in the rate of loss of H_2O at this stage, suggesting a slowing in the radiolytic breakdown of water. This breakdown occurs from the primary interactions of the radiation with water (Equation 2-2) which slows down for two reasons: (1) The dose rate is decreasing over time and (2) The fraction of the radiation energy associated with the water primary events decreases as the fraction of water vapour in the gas phase decreases (Equation 2-26). Also, as H_2O_2 and H_2 accumulate in the system back reactions to reform water become more important. In addition, towards the end of the operational period some loss of HNO_3 is observed, matched by the formation of nitrous acid. This formation followed by subsequent loss of nitric acid from irradiation of moist air mixtures had been noted in the laboratory by Jones (1959).

Figure 4-13 compares the nitric acid production for the present case with that for Case 1 in which 600 g of water were initially present in the canister. The amount of nitric acid produced at steady state is less in the current calculation, by approximately a factor of 2, although the water is roughly a factor of 10 less. The important initial species controlling the amount of nitric acid is O_2, which of course is the same for cases 4 and 1.

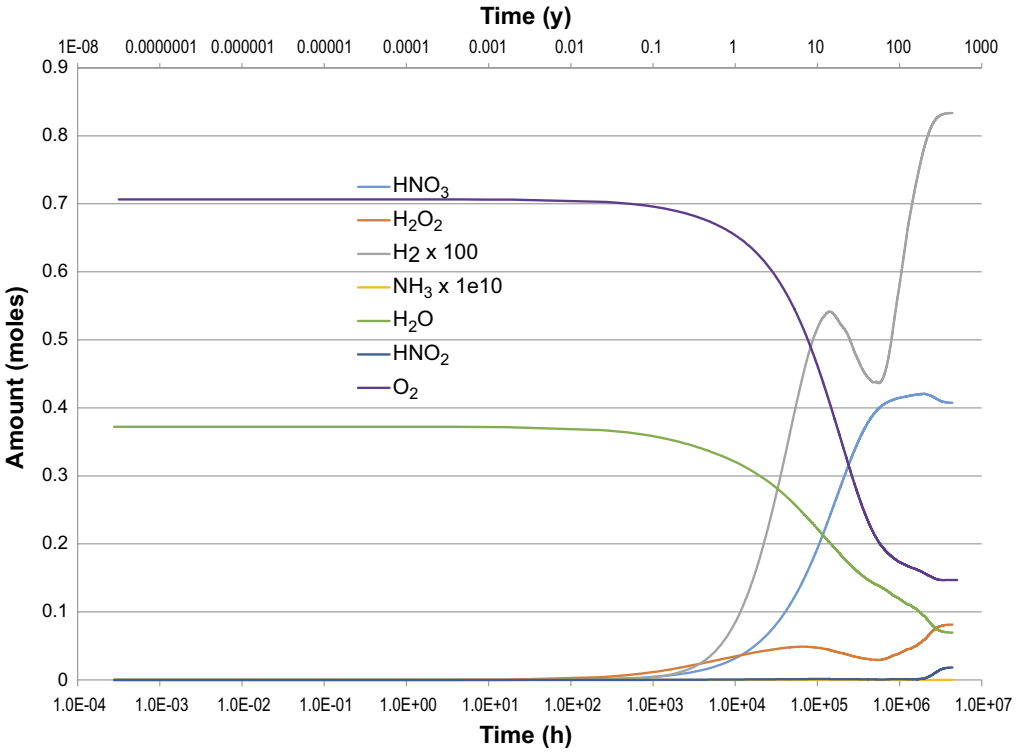

Figure 4-12. *Calculated amounts of main species for Case 4, 6.7 g of water/no corrosion.*

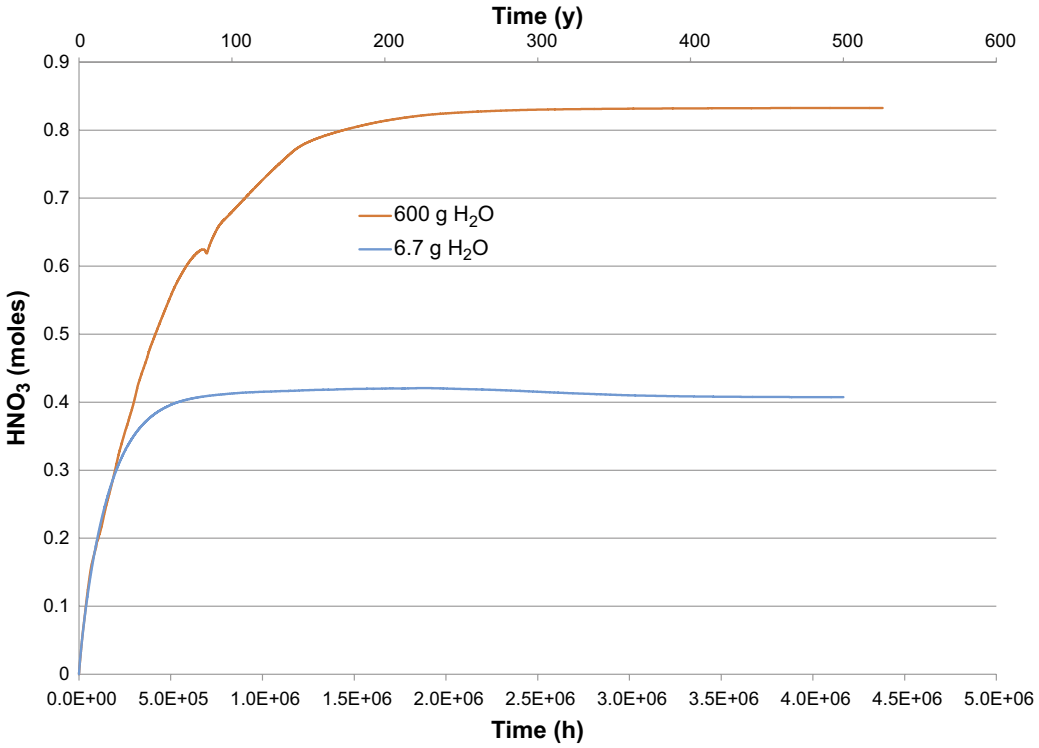

Figure 4-13. *Calculated amounts of nitric acid for Cases 1 and 4, 600 and 6.7 g of water/no corrosion.*

4.2.5 Case 5 – low water content with steel corrosion

Case 5 uses the same initial conditions as Case 4 but now includes aerobic and anaerobic corrosion. Figure 4-14 shows the behaviour of the major gas phase species as a function of time.

Nitric acid, peroxide and H_2 accumulate during the short initial period while corrosion occurs. Most of the water is removed by the aerobic corrosion process, Equation 2-46, repeated here.

$$4Fe + 2H_2O + 3O_2 = 4FeOOH$$

This ceases when oxygen levels are below a threshold of approximately 1 ppm. There is still a small residual amount of water present at this stage that undergoes anaerobic corrosion and radiolysis, reducing the water present further and generating H_2, via reaction 2-47. This is not apparent in Figure 4-10 because of the y-axis scales, but is clearer in Figure 4-15 which plots the same data for H_2 and H_2O on different scales for the first 10^4 h of canister operation.

The behaviour of peroxide and nitric acid largely reflect the consequences of the corrosion processes, increasing while a significant amount of O_2 and H_2O is present in the system but then decreasing as both O_2 and H_2O are removed and H_2 is generated. The relative amounts of these species are small though, $< 2 \times 10^{-4}$ mole, equivalent to a concentration of 2×10^{-7} molar in the canister gas volume of 1 m^3. It should also be noted that very little ammonia is produced under these conditions.

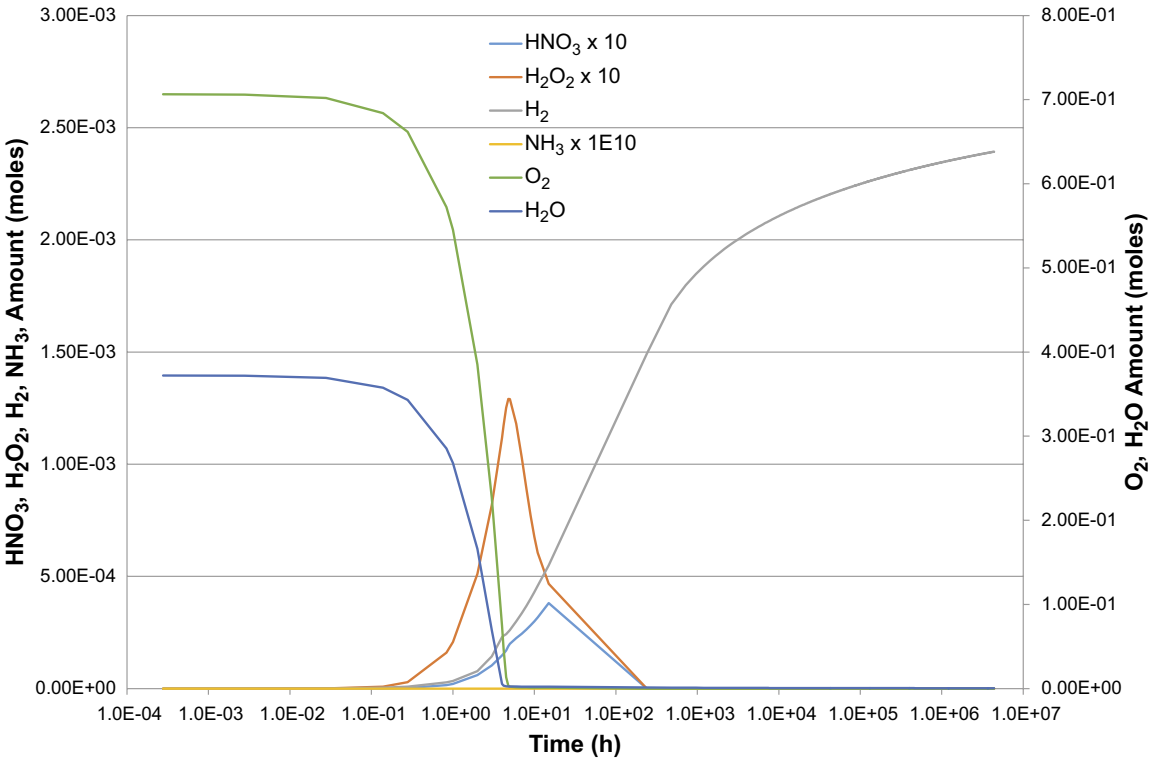

Figure 4-14. *Calculated amounts of major species for Case 5, 6.7 g of water with corrosion.*

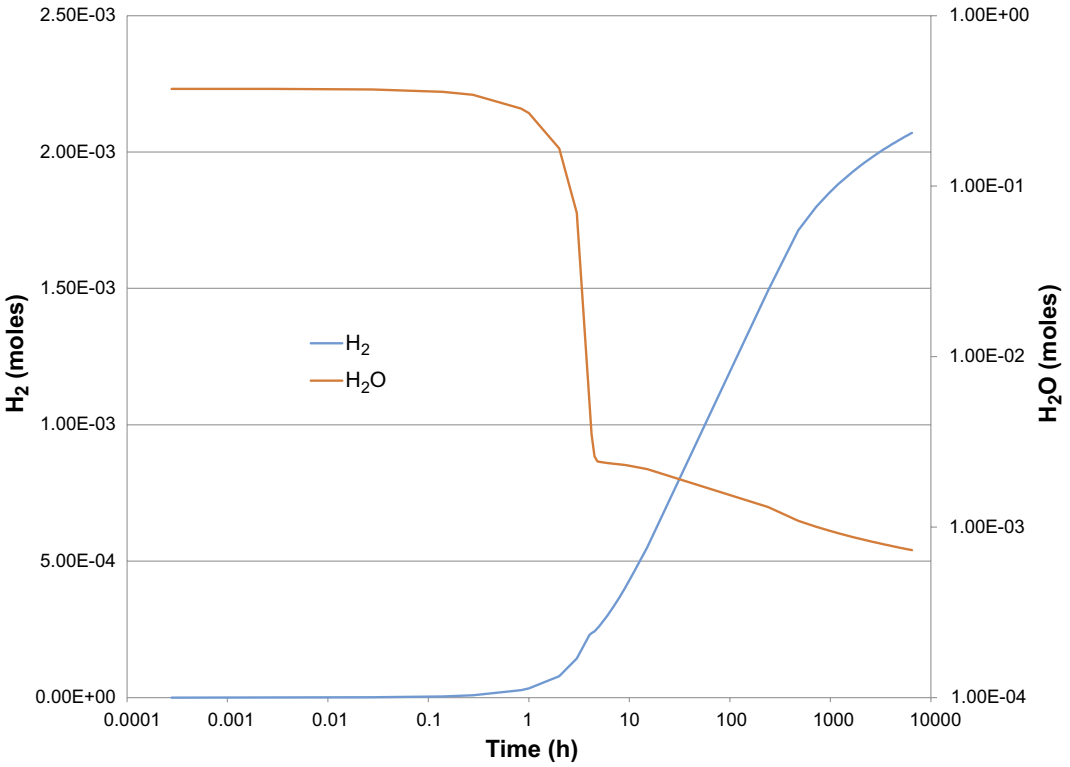

Figure 4-15. *Calculated amounts of H_2 and H_2O species for Cases 5, 6.7 g of water with corrosion.*

4.2.6 Case 6 – low water content with low aerobic steel corrosion rate

For this scenario the steel oxic corrosion rate has been reduced by half, all other initial conditions are identical to Case 5. Figure 4-16 plots the main species as a function of time.

The results presented in Figure 4-16 are very similar to those in Figure 4-14 for Case 5, for the same conditions at the higher aerobic corrosion rate. The lower corrosion rate leads to higher peak peroxide and nitric acid concentrations, as observed for Case 3 compared to Case 2.

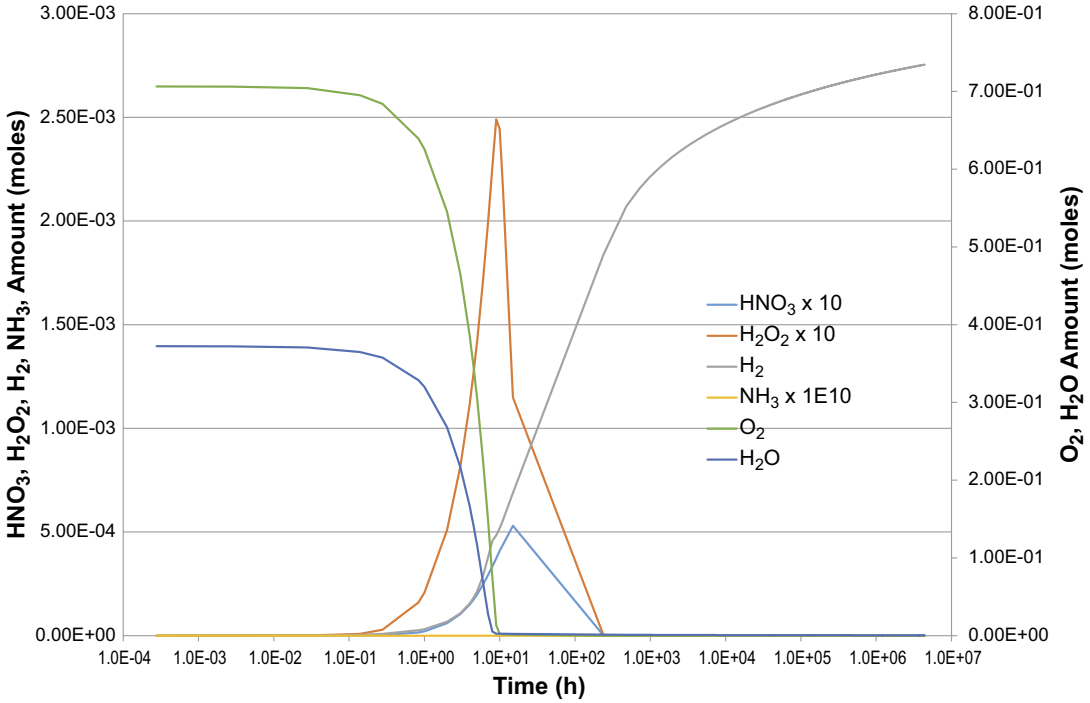

Figure 4-16. *Calculated amounts of major species for Cases 6, 6.7 g of water with corrosion, low aerobic corrosion rate.*

4.2.7 Case 7 – intermediate water content with no steel corrosion rate

This particular calculation was very difficult to get to converge, requiring multiple resetting's of the integration step size and integration accuracy. A reconfiguration of the Jacobian matrix was also required missing out certain inter-dependencies in the equations. After many attempts using a varying temperature/time profile had to be abandoned and the simulation only worked for a constant temperature, taken as 85 ºC, throughout the canister operational period. Prior calculations for Case 1 using a constant temperature suggested this made an approximate 5–10 % difference in the predicted behaviour. Even with this approximation the calculation took over 12 h on a standard PC with an Intel Pentium 7 processor, most of the other calculations presented here took 1–60 minutes.

Figure 4-17 shows the calculated main species concentrations against time for this Case that used 244 g of water and had no corrosion occurring in the canister. The fluctuations in species concentrations around 10^6 h are a consequence of the numerical instabilities mentioned above and are not a consequence of any physical processes in the model. The results are in fact very similar to Case 1 (Figure 4-5), despite the numerical problems, and it is somewhat puzzling why the model should be fine when the input water concentrations are 600 and 6.7 g, but run into problems at 244 g. Nitric acid amounts are between 0.8 and 0.9 moles, with 1.5–2 moles of H_2O_2, some H_2 is produced but very little NH_3 is formed over the 500 year operational period simulated. These results are very similar to Case 1.

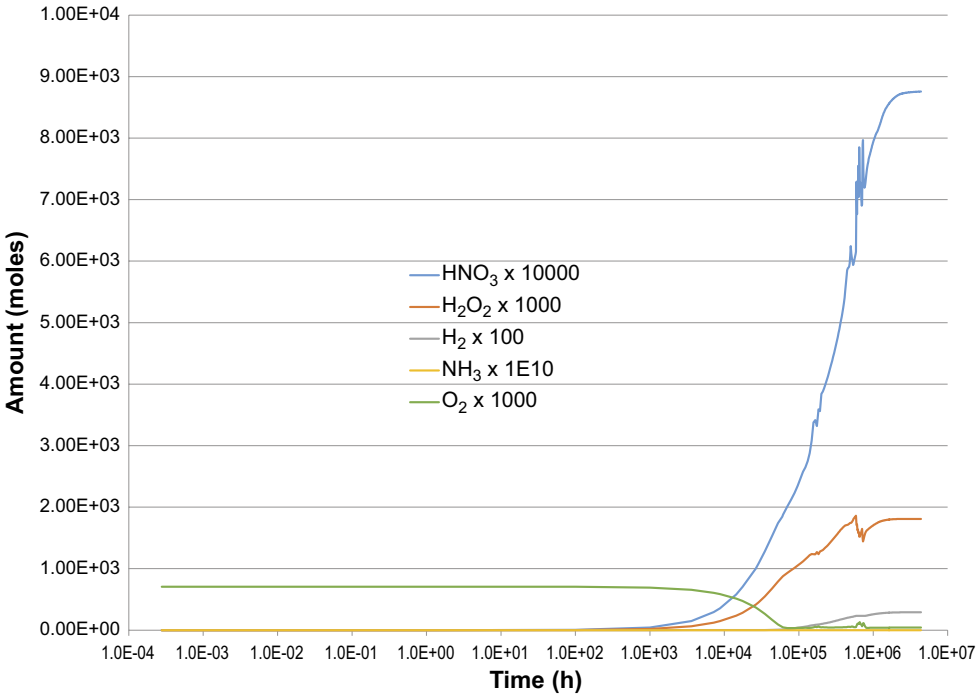

Figure 4-17. *Species concentrations versus time for case 7, intermediate water content, no corrosion.*

4.2.8 Cases 8 and 9 – intermediate water content with steel corrosion

Case 8 is the same initial conditions as Case 7 but including corrosion of the steel. It is interesting that despite this problem involving more differential equations than Case 7, it is numerically more stable and therefore the equations could be solved using the canister temperature profile in Figure 4-2. Figure 4-18 shows the main species concentrations as a function of time.

The introduction of corrosion and the consequent removal of O_2 and H_2O from the system, coupled to the production of H_2, has significantly reduced the amount of nitric acid produced, from 0.8–0.9 moles in the absence of corrosion to values $< 2 \times 10^{-5}$ moles when corrosion occurs. After 500 years of canister operation, the two main components of the gas phase (other than Ar and N_2) are NH_3 and H_2. Note the rise in the gas phase water concentration at around 10^2–10^3 h is a consequence of the vaporisation of the remaining liquid water in the system at this point from the temperature increase. There is also a change from water removal by aerobic corrosion to the slower water removal by anaerobic oxidation during this period.

Figure 4-19 is the equivalent plot to Figure 4-18 for Case 8, identical to 8 except for the lower aerobic corrosion rate.

Lowering the aerobic corrosion rate means it takes longer to remove O_2 (although not obvious on the log scale used) and a consequent increase in the peak HNO_3 concentration compared to Case 8. The final products after 500 y of canister operation are again H_2 and NH_3 at very similar values for those of Case 8.

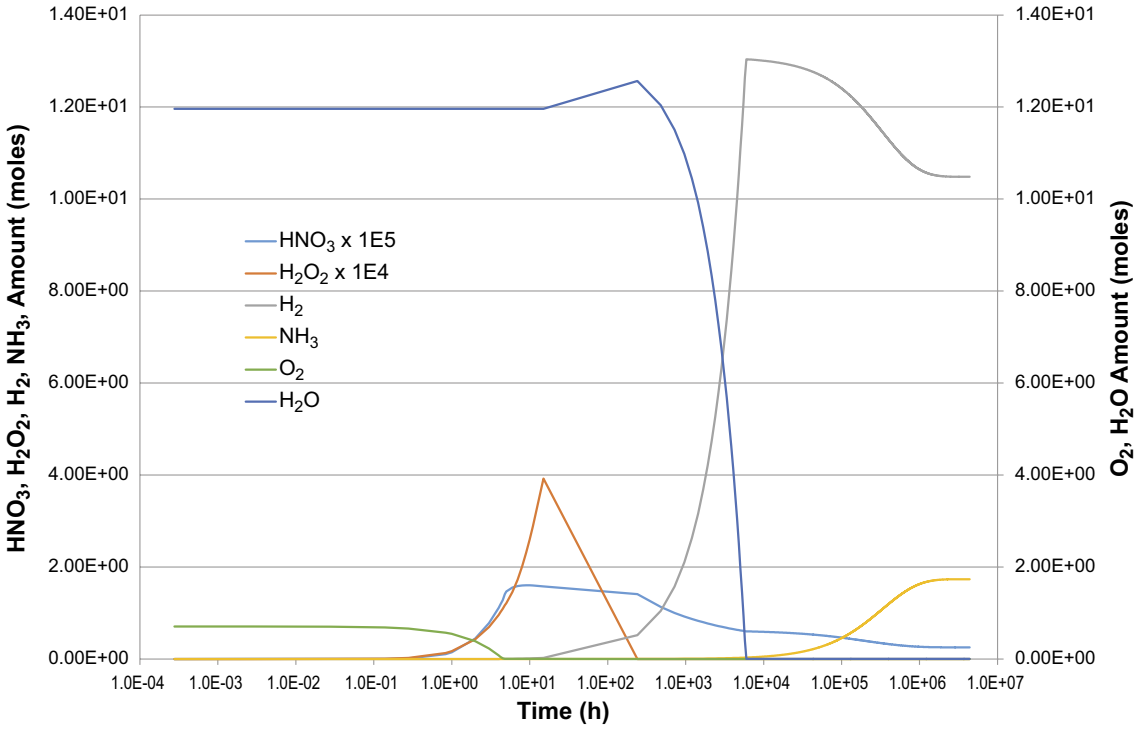

Figure 4-18. *Species concentrations versus time for case 8, intermediate water content, with corrosion.*

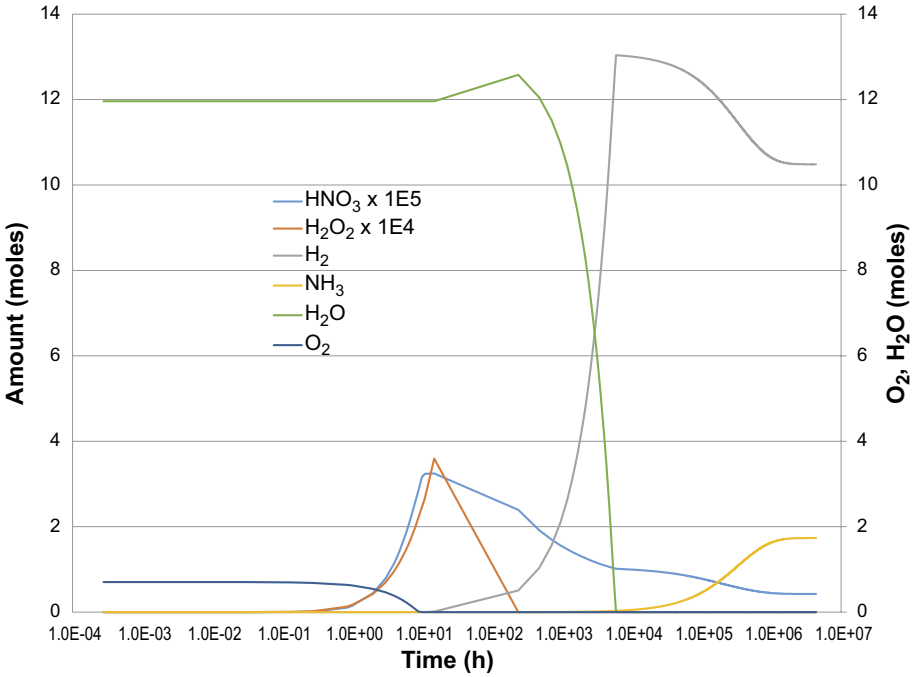

Figure 4-19. *Species concentrations versus time for case 9, intermediate water content, with low corrosion rate.*

4.2.9 Case 10 – high water content with no steel corrosion and low air content

Case 10 is analogous to Case 1 in which there is a large volume of water in the canister and no corrosion taking place, however only 1 % air is initially present, not 10 % as assumed for Case 1. This case also proved very difficult to converge and this is observed in several discontinuities in the calculated species amounts. Figure 4-20 is a plot of the main species amounts against time for this case, along with the equivalent plots for Case 1 (same scaling factors).

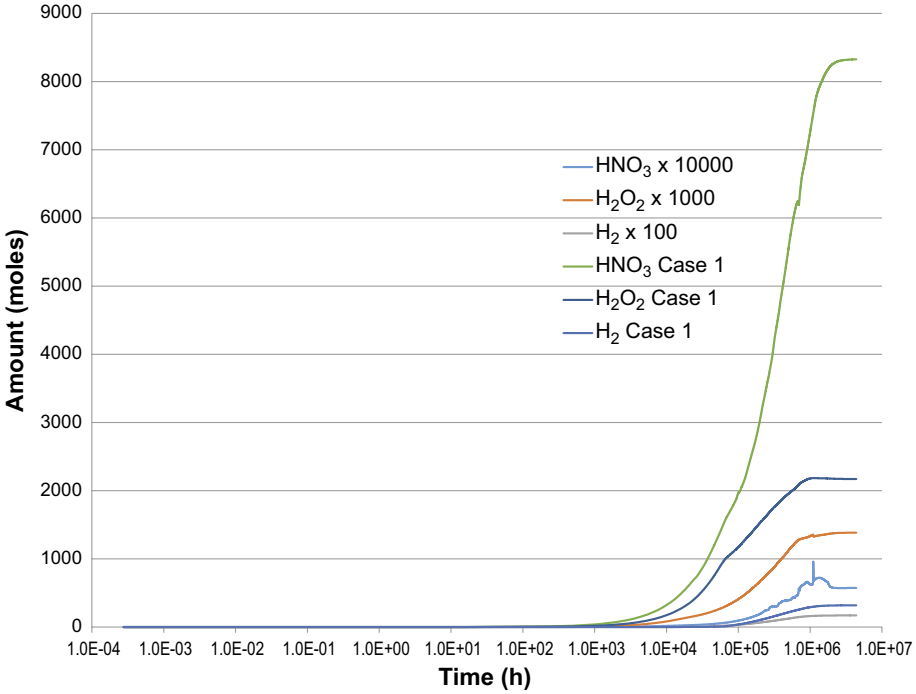

Figure 4-20. *Species concentrations versus time for Case 10, high water content, low air and no corrosion. Also presented are the Case 1 results (high air) using the same scaling factors.*

It is clear that lower the amount of air in the system has led to a drop in all three species concentrations, HNO_3, H_2O_2 and H_2 (there is very little NH_3). The nitric acid concentration has dropped by approximately a factor of 10, roughly in proportion to the fall in air content.

4.2.10 Case 11 – high water content with steel corrosion and low air content

This case is analogous to Case 2, high water content with steel corrosion but here the air content of the canister has been reduced to 1 %. Figure 4-21 shows the results of the calculation for Case 11, plotting the main species concentrations versus time, also plotted are the Case 2 results. The amount of nitric acid produced has fallen substantially (compared to Case 10), while the amount of peroxide has increased, the amount of H_2 has roughly remained constant and the amount of NH_3 has fallen. Since HNO_3 is largely formed from NO_2 + OH and the formation of NO_2 is from a sequence of reactions involving O_2 and O, given that there is less O_2 in Case 11 then Case 2, the lower nitric acid amount is expected. A lower OH+NO_2 rate due to low NO_2 makes more OH available to produce H_2O_2, OH + OH + M = H_2O_2, hence the increase in peroxide. H_2 is largely produced from anaerobic corrosion from water so apart from the fact that this begins earlier as O_2 is removed by aerobic corrosion, little effect of the low air content would be expected, as observed. Finally, the lower NH_3 concentration in Case 11 compared to Case 2 is a consequence of the lower initial N_2 amount in the system.

It should be noted that unlike Case 2, in Case 11 all the water is lost before NH_3 starts to be produced.

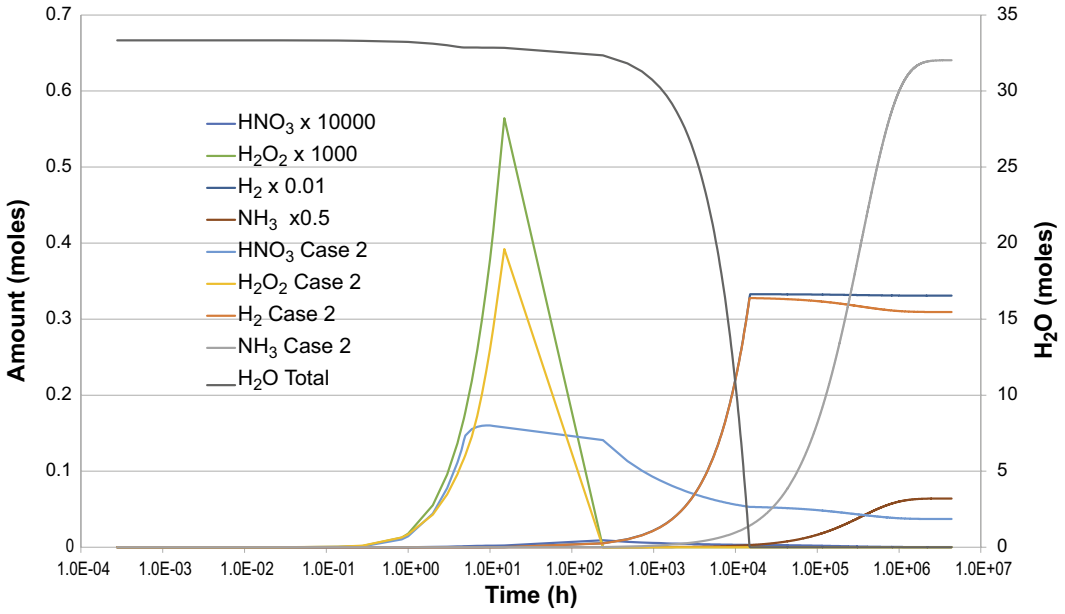

Figure 4-21. *Species concentrations versus time for Case 11, high water content, low air, with corrosion. Also presented are the Case 2 results (high air) using the same scaling factors.*

4.2.11 Cases 12 and 13 – intermediate water content without/with steel corrosion and low air content

Cases 12 and 13 are analogues of Cases 7 and 8, intermediate water content in the canister, without and with steel corrosion, but as for 10 and 11 the air content was just 1 %. Figures 4-22 and 4-23 are plots of species concentrations versus time for Cases 12 and 13. Also plotted are the results for analogous Cases 7 and 8 at the higher initial air concentrations. For case 12 there is a fall in all species concentrations as a consequence of the lower air content, nitric acid falling by approximately a factor of 10 compared to Case 7. For Case 13 the behaviour is very similar to Case 11, the nitric acid and ammonia concentrations are significantly lower in Case 13 compared to the equivalent Case 8, but peroxide is higher. The reasons for this behaviour have already been provided above.

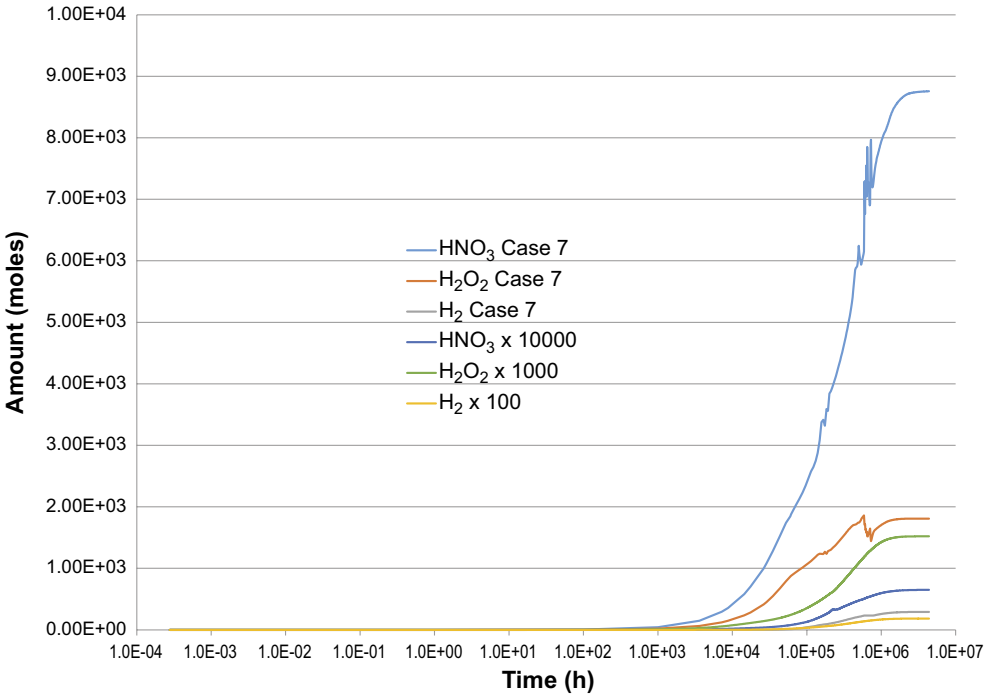

Figure 4-22. *Species concentrations versus time for Case 12, intermediate water content, low air, without corrosion. Also presented are the Case 7 results (high air) using the same scaling factors.*

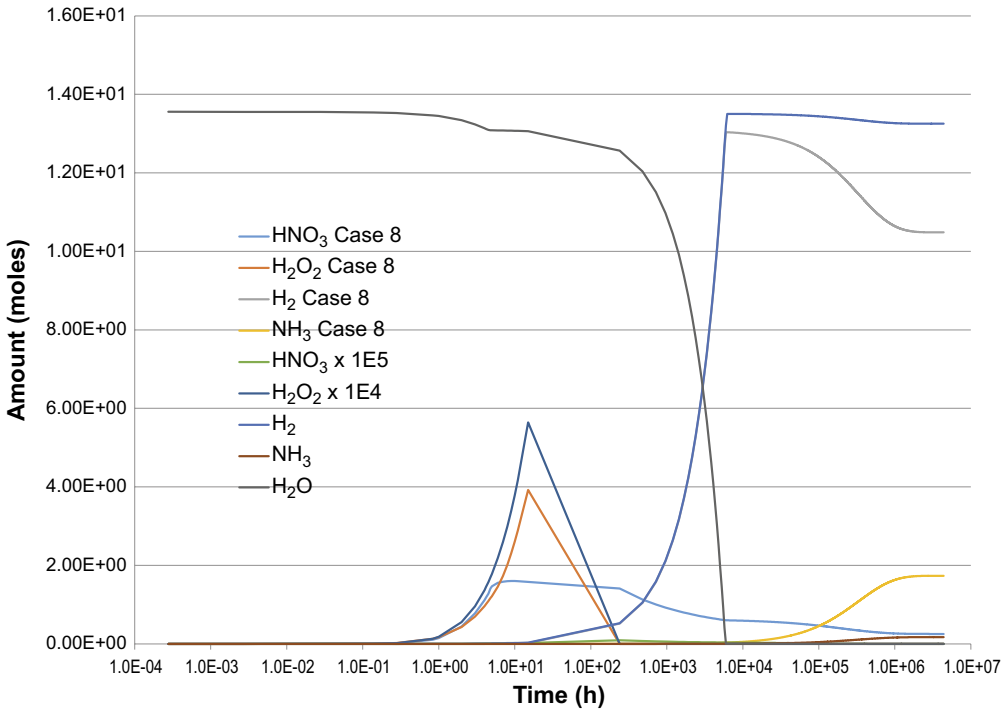

Figure 4-23. *Species concentrations versus time for Case 13, intermediate water content, low air, with corrosion. Also presented are the Case 8 results (high air) using the same scaling factors.*

4.2.12 Cases 14 and 15 – low water content without/with steel corrosion and low air content

The results of these calculations are given in Figures 4-24 and 4-25, in which the analogous high air cases (Cases 4 and 5) are also provided. Figure 4-19, the cases where no corrosion is occurring in the system, the expected fall in species concentrations is observed in the low air case.

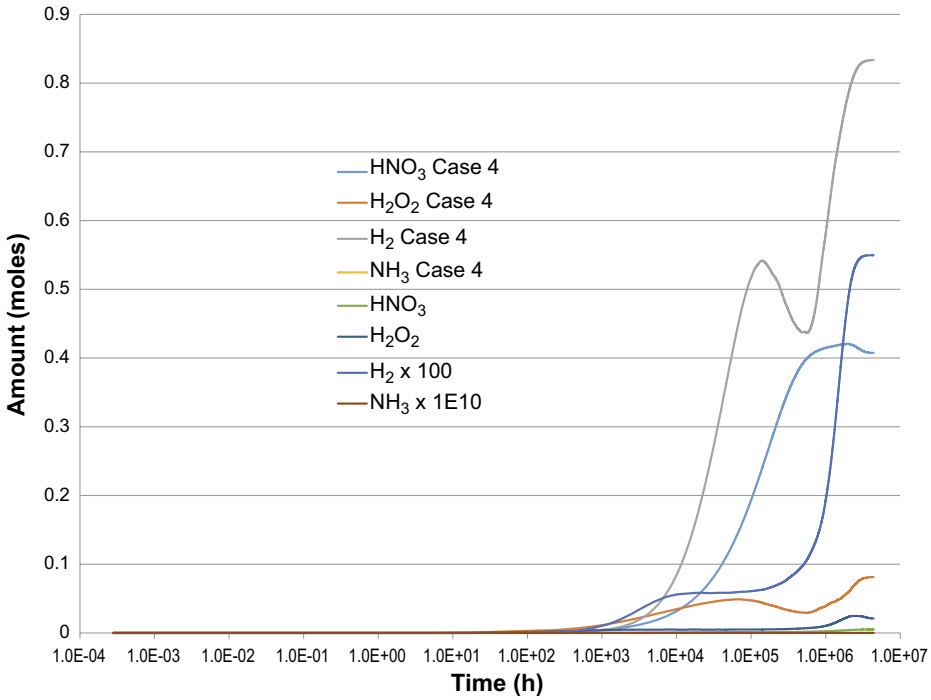

Figure 4-24. *Species concentrations versus time for Case 14, low water content, low air, without corrosion. Also presented are the Case 4 results (high air) using the same scaling factors.*

Figure 4-25 is interesting in that in the high air case very little NH_3 is calculated but NH_3 is formed in the low air case, with the subsequent loss of H_2. The reason for this is that in the high air case, H_2O is removed by aerobic oxidation with little H_2 production and subsequent NH_3 formation. In the low air case, once aerobic oxidation ceases some H_2O remains for subsequent anaerobic oxidation, H_2 production and finally NH_3 formation.

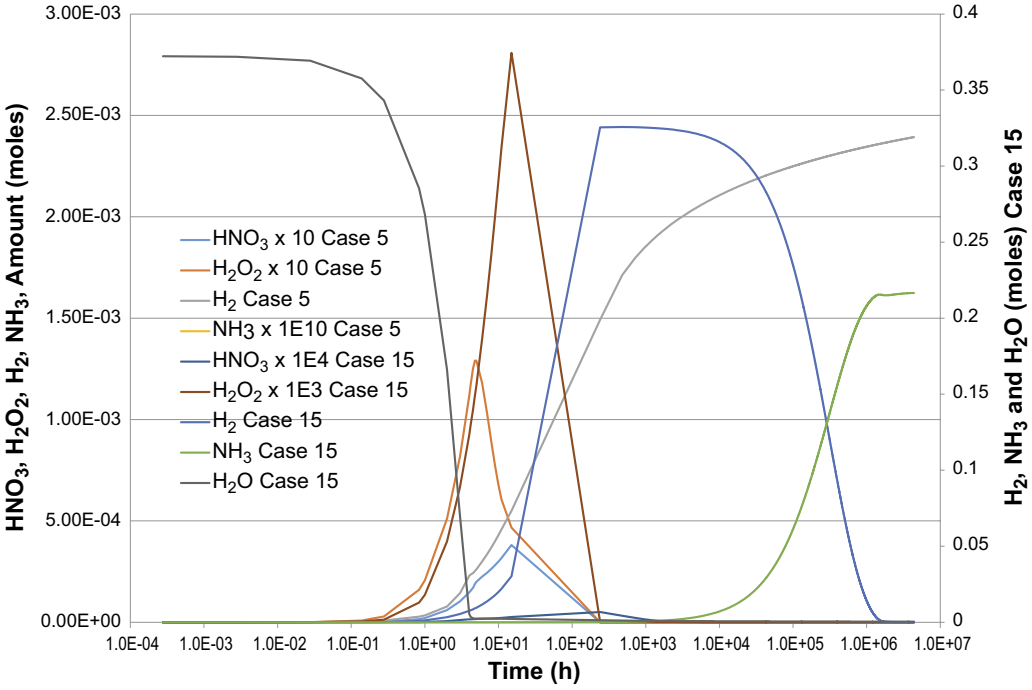

Figure 4-25. *Species concentrations versus time for Case 15, low water content, low air, with corrosion. Also presented are the Case 5 results (high air) using the same scaling factors.*

5 Discussion

This report describes a new model for the gas phase chemistry taking place inside the KBS-3 fuel storage canister. The model simulates the radiolysis chemistry of Ar-O_2-N_2-H_2O gas mixtures as a consequence of the radiation field inside the canister, along with vaporisation/condensation of H_2O, as well as aerobic and anaerobic corrosion of the iron present. This new model is similar to a model used previously by Henshaw et al. (1990) and Henshaw (1994) to describe this system but contains more extensive chemistry and up to date chemical kinetic data. The earlier model also did not include vaporisation/condensation of water, it simply assumed an initial water vapour pressure inside the canister, it also did not include the effects of corrosion, which removes O_2 and H_2O and produces H_2. The new model solves the 300–400 ordinary differential equations describing the system, starting from the initially defined conditions, to predict gas phase species concentrations as a function of time. Simulations have been performed for the first 500 years of the canister operation, which is generally long enough for species concentrations to reach a steady state.

In order to validate the model, calculations were performed to simulate the experimental results of May et al. (1976), Jones (1959), Linacre and Marsh (1981), Tokunaga and Suzuki (1984) and Cheek and Linnenbom (1958). These workers irradiated various relevant gas mixtures using either electron beams or gamma irradiators and measured gas phase species concentrations as a function of dose. The model:

- Gave a G-value for nitric acid production from irradiation of moist air of 1.9, close to the experimental value of 2 obtained by May et al. (1976) and Jones (1959);
- Accounted for the apparent increase in nitric acid production rate from the presence of Ar, as described by Linacre and Marsh (1981);
- Simulated reasonably well the nitrogen oxide and nitric acid production results of Tokunaga and Suzuki (1984);
- Accounted for the formation behaviour of NH_3, including its suppression by the presence of O_2, as observed by Cheek and Linnenbom (1958), although in general the model overestimated the rate of production of ammonia.

These comparisons gave reasonable confidence that the model could be applied to the KBS-3 canister environment and provide reasonable values for the levels of species such as HNO_3 and NH_3 in the system.

The model was applied to the KBS-3 canister and species concentrations calculated for a period of 500 years. Fifteen different sets of initial conditions were chosen, including a high water content (600 g) in the canister, corresponding to multiple failed fuel pins containing water, down to a low water content, 6.7 g, corresponding approximately to the amount of residual water in a canister with one damaged and dried fuel rod. Calculations were performed for high residual air (10 % air) and low residual air (1 %), and either included the effects of corrosion or not. The temperature and dose rate during the calculation also vary with time and are based on reasonable estimates of these quantities, as discussed. The results of the calculations have been provided and discussed in the body of this report, but are summarised in Table 5-1 which gives the species amounts (in moles) at the end of the calculation period of 500 y for each of the cases.

Table 5-1. Calculated species amounts (in moles) at 500 years of canister operation for each of the 15 cases studied.

Case	Description	HNO_3	NH_3	H_2O_2	H_2	O_2
1	high H_2O, high air, no corrosion	8.3×10^{-1}	1.0×10^{-37}	2.17	3.2	5.8×10^{-2}
2	high H_2O, high air, corrosion	3.7×10^{-6}	1.28	1.0×10^{-12}	30.9	9.3×10^{-15}
3	high H_2O, high air, low corrosion	6.3×10^{-6}	1.28	1.7×10^{-12}	30.9	1.6×10^{-14}
4	low H_2O, high air, no corrosion	4.1×10^{-1}	3.2×10^{-4}	8.1×10^{-2}	8.3×10^{-3}	1.5×10^{-1}
5	low H_2O, high air, corrosion	3.6×10^{-15}	2.9×10^{-22}	2.9×10^{-22}	2.4×10^{-3}	3.3×10^{-17}
6	low H_2O, high air, low corrosion	3.5×10^{-15}	1.2×10^{-25}	2.1×10^{-22}	2.8×10^{-3}	1.9×10^{-17}
7	intermediate H_2O, high air, no corrosion	8.8×10^{-1}	1.1×10^{-37}	1.81	2.97	4.3×10^{-2}
8	intermediate H_2O, high air, corrosion	2.5×10^{-6}	1.73	4.1×10^{-13}	10.5	9.9×10^{-15}
9	intermediate H_2O high air, low corrosion	4.3×10^{-6}	1.73	6.8×10^{-13}	10.5	1.6×10^{-14}
10	high H_2O, low air, no corrosion	5.7×10^{-2}	8.0×10^{-40}	1.38	1.7	1.2×10^{-1}
11	high H_2O, low air, corrosion	3.3×10^{-8}	1.3×10^{-1}	5.7×10^{-16}	33	3.1×10^{-17}
12	intermediate H_2O, low air, no corrosion	6.5×10^{-2}	1.8×10^{-39}	1.52	1.83	1.0×10^{-1}
13	intermediate H_2O, low air, corrosion	2.0×10^{-10}	1.7×10^{-1}	2.1×10^{-17}	13.3	6.7×10^{-18}
14	low H_2O, low air, no corrosion	5.1×10^{-3}	1.5×10^{-44}	2.1×10^{-2}	5.5×10^{-3}	5.6×10^{-2}
15	low H_2O, low air, corrosion	4.4×10^{-25}	2.2×10^{-1}	7.6×10^{-22}	1.9×10^{-6}	6.5×10^{-26}

The results in the table (and in the main body of the report) demonstrate:

- In the absence of corrosion significant quantities of nitric acid can be produced. For 600 g of water and 10 % air (Case 1), this amounts to 0.83 moles of HNO_3 along with significant amounts of other oxidising agents, 2.2 moles of H_2O_2 and 0.06 moles O_2. These fall as the water content in the canister decreases, but even at 6.7 g of water (Case 4), 0.4 moles of HNO_3 is produced.
- The inclusion of corrosion effects in the model drastically reduces the amount of nitric acid predicted to be formed. For the case with high water (600 g) and high oxygen (10 % air), the nitric acid falls from 0.83 moles at the end of the 500 y simulation period with no corrosion (Case 1) to 3.7×10^{-6} moles when corrosion is accounted for (Case 2). This occurs for two reasons: (1) the rapid removal of O_2 by aerobic corrosion during the period of high dose rate means the rate of formation of nitrogen oxides, precursors to nitric acid formation, drops dramatically and (2) later anaerobic corrosion leads to relatively large amounts of H_2 in the system that prevent nitrogen oxidation.
- When corrosion is included in the model the final gaseous state can be relatively reducing with large amounts of H_2 and NH_3 present for initial high water content. For example, in Cases 2 (600 g water) and 8 (244 g), 1.3 and 1.7 moles of NH_3 are produced, but at low enough water (6.7 g, Case 5) very little of HNO_3, H_2O_2, NH_3 and H_2 are predicted to form. This is because at low water/high air conditions all the water is removed during aerobic corrosion, not producing H_2. At high water content residual water remains after aerobic corrosion has finished, this leads to H_2 production from anaerobic oxidation and finally to NH_3 via radiolysis.
- A 50 % fall in the aerobic corrosion rate leads to an increase in the amount of nitric acid produced, although the absolute amount is still small, see Cases 2 and 3. There is virtually no effect on the levels of NH_3 and H_2 in the system (see Cases 2 and 3).
- Decreasing the amount of air in the system leads to a lower calculated amount of nitric acid. For Case 1 (600 g H_2O, 10 % air, no corrosion) the amount of nitric acid is 0.83 moles, while at 1 % air (Case 10) only 0.06 moles of HNO_3 are produced. Reducing the air content also reduces the amount of ammonia formed (less N_2 available), so for Case 2 (600 g H_2O, 10 % air) for example 30.9 moles of H_2 and 1.28 moles of NH_3 are formed, but when the air content is dropped to 1 % (Case 11) 33 moles of H_2 are formed and only 0.13 moles of NH_3. It should be noted that as NH_3 is formed H_2O is consumed, so when the ammonia concentration peaks, no liquid water is present (see Figure 4-7). However, at high air content (10 %) there is a period during which ammonia is forming and water is present in the system (see Figure 4-7), but this is not the case at low air (1 %, see Figure 4-21).

The model developed and presented here predicts at low water and low amounts of air in the canister that if iron corrosion is taking place very little aggressive species (HNO_3, NH_3) will be produced. Increasing water, increasing air and lowering of the corrosion rates will lead to increasing amounts of HNO_3. There are a number of assumptions used in this model and some phenomena that are not included:

1. That corrosion rates are constant throughout the 500 y operational period. Since most of the impact of corrosion is calculated to occur in the first few years of operation (removing O_2 and H_2O and producing H_2) this assumption is probably not important. It has been demonstrated experimentally that the corrosion rate stays relatively constant over such a period (see Smart and Rance 2005, tests performed for 416 days).
2. It is assumed the corrosion rate is independent of temperature. Although the calculations have not explicitly included the effect of temperature on corrosion rate, sensitivity calculations have been performed on the effect of the aerobic corrosion rate. These calculations suggest ignoring the temperature variation of the corrosion rate is pessimistic: constant aerobic corrosion rates for 70 and 20 °C have been used and anaerobic corrosion rates measured at 30 °C. A linear increase of the aerobic corrosion rate in a closed system (as the KBS-3 canister) with temperature is noted in Figure 4 of Swanton et al. (2015). Instead, here rates corresponding to room temperature corrosion were applied. It is highly likely therefore that at the higher temperatures of the canister corrosion rates will be larger than assumed here, and results here suggest increasing the corrosion rate leads to lower amounts of aggressive species.
3. The model does not include partitioning of soluble gaseous species into the liquid phase. This is probably the primary weakness of the model as gases such as HNO_3 and NH_3 will dissolve in any liquid films present. This would be relevant during the first year and a half after closure. At later stages all of the H_2O initially present has been removed by corrosion, so no solutions of NH_3 will exist. This partitioning process could be included in the model, but this has not been carried out here.
4. The presence of liquid water also means radiolysis processes are occurring in this liquid, these have also not been modelled as part of this study.

Despite these shortcomings the authors believe the model presented here should provide a reasonable representation of the chemistry taking place in the gaseous atmosphere of the KBS-3 canister. Further work on the model would be required to address some of the above shortcomings.

6 Summary

A model has been developed and applied to calculate the amount of nitric acid and ammonia produced inside the gas space of the KBS-3 waste storage canister from gas phase radiolysis of different Ar-Air-Water mixtures. The model was tested by comparisons with laboratory data from a number of irradiation experiments and gave reasonable results. The main conclusions of the report are:

- In the absence of iron corrosion significant amounts of nitric acid may be formed inside the canister;
- The amount of nitric acid formed decreases as the initial air content is reduced;
- The presence of aerobic steel corrosion followed by anaerobic corrosion significantly reduces the amount of nitric acid formed by many orders of magnitude;
- Anaerobic corrosion in the canister may lead to reducing conditions and the formation of ammonia, however, the water initially present in the system is consumed by the corrosion process. When ammonia reaches its peak concentration there is no water in the system. However, at high water content (600 g) and high air (10 %) there is a period when water is present and ammonia is being formed.

There are a number of assumptions in the model and some phenomena taking place inside the canister are not modelled, however it is thought the calculations given here should provide a reasonable estimate of the amounts of radiolysis products (HNO_3, NH_3, H_2O_2 and H_2) present in the system.

References

SKB's (Svensk Kärnbränslehantering AB) publications can be found at www.skb.com/publications. SKBdoc documents will be submitted upon request to document@skb.se.

Bartels D M, Henshaw J, Sims H E, 2013. Modeling the critical hydrogen concentration in the AECL test reactor. Radiation Physics and Chemistry 82, 16–24.

Baulch D L, Drysdale D D, Horne D G, 1973. Evaluated kinetic data for high temperature reactions, Vol. 2. Homogeneous gas phase reactions of the H_2-N_2-O_2 system. London: Butterworths.

Busi F, D´Angelantonio M, Mulazzani Q G, Rafaelli V, Tubertini O, 1987. A kinetic model for radiation treatment of combustion gases. Science of The Total Environment 64, 231–238.

Cheek C H, Linnenbom V J, 1958. Radiation induced formation of ammonia. The Journal of Physical Chemistry 62, 1475–1479.

Curtis A, Sweetenham W, 1987. FACSIMILE User's manual. Harwell Laboratory Report AERE-R12805.

Dmitriev M, 1965. Effects of nuclear and ionizing radiation on the physico-chemical processes affecting nitric acid formation and disintegration in air. Russian Journal of Physical Chemistry 35, 495.

Endo A, Henshaw J, Mignanelli M A, 1996. Computer simulation to predict ozone concentration in an electron accelerator room. Radioisotopes 45, 431–434.

Endo A, Henshaw J, Mignanelli M A, 1998. Time-dependent chemical compositions of ^{13}N and ^{15}O induced in air by the operation of a high energy electron accelerator. Health Physics 74, 456–464.

Gear G W, 1971. Numerical initial value problems in ordinary differential equations. Englewood Cliffs, NJ: Prentice-Hall.

Hartek P, Dondes S, 1964. Radiation chemistry of the fixation of nitrogen. Science 146, 30–35.

Henshaw J, 1994. Modelling of nitric acid production in the Advanced Cold Process Canister due to irradiation of moist air. AEA-D&W 0706/RS3429, AEA Technology, UK (also published as SKB TR 94-15, Svensk Kärnbränslehantering AB).

Henshaw J, Hoch A, Sharland S M, 1990. Further assessment of the advanced cold process canister. AEA-D&R 0060, AEA Technology, UK.

Ibe E, Karasawa H, Nagase M, Endo M, Uchida S, Utamura M, Miki M, 1989. Chemistry of radioactive Nitrogen in BWR primary system. Journal of Nuclear Science and Technology 26, 844–851.

Ikezoe Y, Matsuoka S, Takebe M, Viggiano A (eds), 1987. Gas phase ion-molecule rate constants through 1986. Tokyo: Ion Reaction Research Group of the Mass Spectroscopy Society of Japan.

Jones A R, 1959. Radiation-induced reactions in the N_2-O_2-H_2O system. Radiation Research 10, 655–663.

Kee R J, Rupley F M, Miller J A, Coltrin M E, Grcar J F, Meeks E, Moffat H K, Lutz A E, Dixon-Lewis G, Smooke M D, Warnatz J, Evans G H, Larson R S, Mitchell R E, Petzold L R, Reynolds W C, Caracotsios M, Stewart W E, Glarborg P, Wang C, Adigun O, 2000. CHEMKIN: a software package for the analysis of gas-phase chemical and plasma kinetics. CHE-036-1, CHEMKIN Collection Release 3.6. San Diego, CA.

Linacre J K, Marsh W R, 1981. The radiation chemistry of heterogeneous and homogeneous nitrogen and water systems, AERE-R 10027, UKAEA Atomic Energy Research Establishment.

Manion J A, Huie R E, Levin R D, Burgess Jr D R, Orkin V L, Tsang W, McGivern W S, Hudgens J W, Knyazev V D, Atkinson D B, Chai E, Tereza A M, Lin C-Y, Allison T C, Mallard W G, Westley F, Herron J T, Hampson R F, Frizzell D H, 2015. NIST Chemical Kinetics Database. NIST Standard Reference Database 17, Version 7.0 (Web Version), Release 1.6.8, Data version 2015.09. Gaithersburg, MD: National Institute of Standards and Technology. Available at: https://kinetics.nist.gov/

Marsh G, 1990. A preliminary assessment of the Advanced Cold Process Canister. AEA-InTec-0011, AEA Techonology, UK.

May R, Stinchcombe D, White H, 1976. The radiolytic formation of nitric acid in argon/air/water systems. Harwell Lab. Report AERE-R8179.

Neretnieks I, Johansson A J, 2014. Corrosion of the copper canister inside due to radiolysis of remaining water in the insert. SKBdoc 1419961 ver 1.0, Svensk Kärnbränslehantering AB.

Park J-H, Ahn J-W, Kim K-H, Son Y-S, 2019. Historic and futuristic review of electron beam technology for the treatment of SO_2 and NO_x in flue gas. Chemical Engineering Journal 355, 351–366.

Person J C, Ham D O, 1988. Removal of SO_2 and NO_x from stack gases by electron beam irradiation. Radiation Physics and Chemistry 31, 1–8.

Pilling M J, Smith I W M (eds), 1987. Modern gas kinetics: theory, experiment and application. Oxford: Blackwell Scientific.

SKB, 2006. Long-term safety for KBS-3 repositories at Forsmark and Laxemar – a first evaluation. Main report of the SR-Can project. SKB TR-06-09, Svensk Kärnbränslehantering AB.

SKB, 2010. Design, production and initial state of the canister. SKB TR-10-14, Svensk Kärnbränslehantering AB.

Smart N R, Rance A P, 2005. Effect of radiation on anaerobic corrosion of iron. SKB TR-05-05, Svensk Kärnbränslehantering AB.

Speller F, 1951. Corrosion: causes and prevention. 3rd ed. New York: McGraw-Hill.

Spinks J W T, Wood R J, 1990. Introduction to radiation chemistry. 3rd ed. New York: Wiley.

Sridhar N, Cragnolino G A, Dunn D D, Manakhala H H, 1994. Review of degradation modes of alternate container designs and materials. CNWRA-94-010, Center for Nuclear Waste Regulatory Analyses, San Antonio, TX.

Swanton S W, Baston G M N, Smart N R, 2015. Rates of steel corrosion and carbon-14 release from irradiated steels – state of the art review (D2.1). European Commission.

Tsang W, Herron J, 1991. Chemical kinetic database for propellant combustion. 1. Reactions involving NO, NO_2, HNO_3, HNO_2, HCN and N_2O. Journal of Physical and Chemical Reference Data 20, 609–663.

Tokunaga O, Suzuki N, 1984. Radiation chemical reactions in NO_x and SO_2 removals from flue gas. Radiation Physics and Chemistry 24, 145–165.

Uhlig H H, Revie R W, 1985. Corrosion and corrosion control: an introduction to corrosion science and engineering. 3rd ed. New York: Wiley.

Warneck P, 1988. Chemistry of the natural atmosphere. Cambridge, MA: Academic Press.

Willingham C, 1981. Radiation dose rates from commercial PWR and BWR spent fuel elements. PNNL report PNL-3954, Pacific Northwest National Laboratory, Richmond, WA.

Willis C, Boyd A W, 1976. Excitation in the radiation chemistry of inorganic gases. International Journal for Radiation Physics and Chemistry 8, 71–111.

Wittman R, 2013. Radiolysis model sensitivity analysis for a used fuel storage canister. PNNL report 22773, Pacific Northwest National Laboratory, Richmond, WA.

Wood C J, Mascall R A, 1975. Gamma irradiation induced isotopic exchange in nitrogen sensitized by helium, neon and argon. Journal of the Chemical Society, Faraday Transactions 71, 1678–1688.

Woodall J, Agúndez M, Markwick-Kemper A J, Millar T J, 2007. The UMIST database for astrochemistry 2006. Astronomy & Astrophysics 466, 1197–1204 (see UMIST, http://udfa.ajmarkwick.net/).

Acknowledgements

The authors would like to thank Thomas Bergander of SKB for sponsoring this work. We also dedicate this report to the late Lars Werme who instigated this area of research back in 1989 and enthusiastically supported our earlier studies.

Appendix

Chemical reaction set used in model

Number	Reaction
1	$N_2 = N_2^+ + e^-$
2	$N_2 = N^+ + e^- + N$
3	$N_2 = N + N$
4	$N_2 = ND2 + ND2$
5	$N_2 = NP2 + NP2$
6	$N_2 = N_2^*$
7	$O_2 = O_2^+ + e^-$
8	$O_2 = O^+ + e^- + O$
9	$O_2 = O_2^*$
10	$H_2O = H_2O^+ + e^-$
11	$H_2O = H + OH$
12	$H_2O = OH + H^+ + e^-$
13	$H_2O = O + H^+ + H^+ + e^- + e^-$
14	$H_2O = O + H_2$
15	$Ar = Ar^+ + e^-$
16	$Ar = Ar^*$
17	$NH_3 = NH_3^+ + e^-$
18	$NH_3 = NH_2^+ + H + e^-$
19	$NH_3 = NH^+ + H_2 + e^-$
20	$NH_3 = NH^+ + H + H + e^-$
21	$NH_3 = NH_2 + H$
22	$NH_3 = NH + H_2$
24	$N2^* + M = N_2 + M$
25	$N2^* + NO = NO + N2$
26	$N2^* + O_2 = O + O + N_2$
27	$N2^* + N_2O = N_2 + N_2 + O$
28	$N2^* + NO_2 = NO + O + N_2$
29	$O_2^* + M = O_2 + M$
30	$H^+ + H_2O = H_3O^+$
31	$H_2O^+ + H_2O = H_3O^+ + OH$
32	$H_2O^+ + O_2 = O_2^+ + H_2O$
33	$N_3^+ + O_2 = NO^+ + N_2O$
34	$N_3^+ + O_2 = NO_2^+ + N_2$
35	$N_3^+ + NO = NO^+ + N + N_2$
36	$N_3^+ + NO_2 = NO^+ + NO + N_2$
37	$N_3^+ + NO_2 = NO_2^+ + N + N_2$
38	$N_3^+ + N_2O = NO^+ + N_2 + N_2$
39	$N_3^+ + e^- = N + N_2$
40	$N_3^+ + NO_2^- = N + N_2 + NO_2$
41	$O^+ + N_2 = NO^+ + N$
42	$O^+ + NO = NO^+ + O$
43	$O^+ + O_2 = O_2^+ + O$
44	$O^+ + NO_2 = NO_2^+ + O$
45	$O^+ + NO_2^- = O + NO_2$
46	$O_2^+ + NO = NO^+ + O_2$
47	$O_2^+ + NO_2 = NO_2^+ + O_2$
48	$O_2^+ + e^- = O_2$

Number	Reaction
49	$O_2^+ + NO_2^- = O_2 + NO_2$
50	$NO_2^+ + NO = NO^+ + NO_2$
51	$NO_2^+ + e^- = NO + O$
52	$NO_2^+ + e^- = NO_2$
53	$NO_2^+ + NO_2^- = NO_2 + NO_2$
54	$NO_2^+ + NO_3^- = NO_2 + NO_3$
55	$N_2^+ + NO = NO^+ + N_2$
56	$N_2^+ + NO_2 = NO_2^+ + N_2$
57	$N_2^+ + NO_2 = NO^+ + N_2O$
58	$N_2^+ + e^- = N + N$
59	$N_2^+ + e^- = N_2$
60	$N_2^+ + NO_2^- = N_2 + NO_2$
61	$N_2^+ + NO_3^- = N_2 + NO_3$
62	$N_2^+ + O_2^- = N_2 + O_2$
63	$N_2^+ + O_2 = O_2^+ + N_2$
64	$N_2^+ + H_2O = H_2O^+ + N_2$
65	$N_2^+ + H_2O_2 = H_2O_2^+ + N_2$
66	$NO_2^+ + H_2O_2 = H_2O_2^+ + NO_2$
67	$H_2O_2^+ + e^- = OH + OH$
68	$H_2O_2^+ + NO_2^- = OH + OH + NO_2$
69	$H_2O_2^+ + NO_3^- = OH + OH + NO_3$
70	$H_2O_2^+ + O_2^- = OH + OH + O_2$
71	$N_2^+ + N_2 + M = N_4^+ + M$
72	$N_2^+ + H_2 = HN_2^+ + H$
73	$NO^+ + e^- = N + O$
74	$NO^+ + e^- = N + O$
75	$NO^+ + e^- = NO$
76	$NO^+ + NO_2^- = NO + NO_2$
77	$NO^+ + NO_3^- = NO + NO_3$
78	$NO^+ + O_2 + M = NO^+O_2 + M$
79	$NO^+O_2 + NO_2^- = NO + O_2 + NO_2$
80	$NO^+O_2 + NO_2^- = NO_3 + NO_2$
81	$NO^+O_2 + NO_3^- = NO + O_2 + NO_3$
82	$NO^+O_2 + e^- = NO + O_2$
83	$N^+ + N_2 + M = M + N_3^+$
84	$N^+ + O_2 = NO^+ + O$
85	$N^+ + O_2 = O_2^+ + N$
86	$N^+ + O_2 = O^+ + NO$
87	$N^+ + NO = NO^+ + N$
88	$N_4^+ + NO = NO^+ + N_2 + N_2$
89	$N_4^+ + NO_2 = NO_2^+ + N_2 + N_2$
90	$N_4^+ + NO_2 = NO^+ + N_2O + N_2$
91	$N_4^+ + O_2 = O_2^+ + N_2 + N_2$
92	$N_4^+ + e^- = N_2 + N_2$
93	$N_4^+ + e^- = N + N + N_2$
94	$N_4^+ + NO_2^- = NO_2 + N_2 + N_2$
95	$N_4^+ + NO_3^- = NO_3 + N_2 + N_2$
96	$NH_4^+ + e^- = NH_2 + H_2$
97	$NH_4^+ + e^- = NH_2 + H + H$
98	$NH_3^+ + e^- = NH_2 + H$
99	$NH_3^+ + e^- = NH + H + H$

Number	Reaction
100	$NH_3^+ + NH_3 = NH_4^+ + NH_2$
101	$NH_2^+ + e^- = N + H + H$
102	$NH_2^+ + NH_3 = NH_3^+ + NH_2$
103	$NH^+ + e^- = N + H$
104	$O_2^+ + H_2O + M = O_2^+H_2O + M$
105	$O_2^+H_2O + H_2O = H_3O^+ + OH + O_2$
106	$H_3O^+ + H_2O + M = H_3O^+H_2O + M$
107	$H_3O^+H_2O + H_2O = H_3O^+H_2O_2$
108	$H_3O^+H_2O + e^- = H + H_2O + H_2O$
109	$H_3O^+H_2O_2 + e^- = H + H_2O + H_2O + H_2O$
110	$H_3O^+H_2O + NO_2^- = H + NO_2 + H_2O + H_2O$
111	$H_3O^+H_2O_2 + NO_2^- = H + NO_2 + H_2O + H_2O + H_2O$
112	$H_3O^+H_2O + NO_3^- = H + NO_3 + H_2O + H_2O$
113	$H_3O^+H_2O_2 + NO_3^- = H + NO_3 + H_2O + H_2O + H_2O$
114	$N_3^+ + H_2O = H_2NO^+ + N_2$
115	$H_2NO^+ + e^- = H_2O + N$
116	$H_2NO^+ + NO_2^- = H_2O + N + NO_2$
117	$H_2NO^+ + NO_3^- = H_2O + N + NO_3$
118	$NO_2 + e^- = NO_2^-$
119	$NO_2^- + HNO_3 = NO_3^- + HNO_2$
120	$NO_3^- + HNO_2 = HNO_3 + NO_2^-$
121	$NO_2^- + NO_2 = NO_3^- + NO$
122	$NO_2^- + N_2O = NO_3^- + N_2$
123	$NO_2^- + N_2O_5 = NO_3^- + NO_2 + NO_2$
124	$NO_2^- + O_3 = NO_3^- + O_2$
125	$NO_3^- + NO = NO_2^- + NO_2$
126	$O_2 + e^- + M = M + O_2^-$
127	$O_2^- + NO_2 = NO_2^- + O_2$
128	$N + NH_3 = NH + NH_2$
129	$OH + NH_3 = NH_2 + H_2O$
130	$O + NH_3 = NH_2 + OH$
131	$NH_3 + H = NH_2 + H_2$
132	$NH_3 + N = NH + NH_2$
133	$NH_2 + H_2 = NH_3 + H$
134	$N + NH_3 = NH + NH_2$
135	$NH_2 + NO = N_2 + H_2O$
136	$NH_2 + NO_2 = N_2O + H_2O$
137	$NH_2 + O = NH + OH$
138	$NH_2 + O_2 = OH + HNO$
139	$NH_2 + H + M = NH_3 + M$
140	$NH_2 + NH_2 = NH_3 + NH$
141	$N + NH_2 = NH + NH$
142	$NH_2 + HNO = NH_3 + NO$
143	$O_2^+ + NH_3 = NH_3^+ + O_2$
144	$NH_3^+ + NH_3 = NH_4^+ + NH_2$
145	$H_3O^+ + NH_3 = NH_4^+ + H_2O$
146	$N^+ + NH_3 = NH_3^+ + N$
147	$N_2^+ + NH_3 = NH_3^+ + N_2$
148	$N_3^+ + NH_3 = NH_3^+ + N + N_2$
149	$N_4^+ + NH_3 = NH_3^+ + N_2 + N_2$
150	$NH + H_2 = NH_2 + H$

Number	Reaction
151	$NH + NH = NH_2 + N$
152	$NH + H = H_2 + N$
153	$NH + NH_2 = NH_3 + N$
154	$NH_3^+ + NO_3^- = NH_3 + NO_3$
155	$NH_4^+ + NO_3^- = NH_3 + H + NO_3$
156	$NO^+ + H_2O + M = M + NO^+H_2O$
157	$NO^+H_2O + H_2O + M = NO^+H_2O_2 + M$
158	$NO^+H_2O_2 + M = NO^+H_2O + H_2O + M$
159	$NO^+H_2O_2 + H_2O = NO^+H_2O_3$
160	$NO^+H_2O_3 + H_2O = HNO_2 + H_3O^+H_2O_2$
161	$NO^+H_2O_2 + e^- = NO + H_2O + H_2O$
162	$Ar^+ + N_2 = Ar + N_2^+$
163	$Ar^+ + O_2 = Ar + O_2^+$
164	$Ar^+ + H_2O = ArH^+ + OH$
165	$Ar^+ + H_2O = Ar + H_2O^+$
166	$Ar^+ + H_2O_2 = Ar + H_2O_2^+$
167	$ArH^+ + H_2O = Ar + H_3O^+$
168	$ArH^+ + N_2 = Ar + HN_2^+$
169	$HN_2^+ + H_2O = N_2 + H_3O^+$
170	$Ar^+ + e^- = Ar$
171	$ArH^+ + e^- = Ar + H$
172	$HN_2^+ + e^- = N_2 + H$
173	$Ar^+ + NO_2^- = Ar + NO_2$
174	$ArH^+ + NO_2^- = Ar + H + NO_2$
175	$HN_2^+ + NO_2^- = N_2 + H + NO_2$
176	$Ar^+ + NO_3^- = Ar + NO_3$
177	$ArH^+ + NO_3^- = Ar + H + NO_3$
178	$HN_2^+ + NO_3^- = N_2 + H + NO_3$
179	$Ar^+ + O_2^- = Ar + O_2$
180	$ArH^+ + O_2^- = Ar + H + O_2$
181	$HN_2^+ + O_2^- = N_2 + H + O_2$
182	$Ar^* + N_2 = N + N + Ar$
183	$Ar^* + O_2 = O + O + Ar$
184	$Ar^* + H_2O = H + OH + Ar$
185	$H_2O^+ + e^- = H + OH$
186	$H_2O^+ + NO_2^- = H + OH + NO_2$
187	$H_2O^+ + NO_3^- = H + OH + NO_3$
188	$H_2O^+ + O_2^- = H + OH + O_2$
189	$H_2O_2^+ + e^- = OH + OH$
190	$H_2O_2^+ + NO_2^- = OH + OH + NO_2$
191	$H_2O_2^+ + NO_3^- = OH + OH + NO_3$
192	$H_2O_2^+ + O_2^- = OH + OH + O_2$
193	$H + O_2 = O + OH$
194	$H + H + M = H_2 + H_2$
195	$H + O_2 + H_2O = HO_2 + H_2O$
196	$H + O_2 + M = HO_2 + M$
197	$OH + OH = H_2O + O$
198	$H + OH + M = H_2O + M$
199	$O_2 + M = O + O + M$
200	$H_2 + O = H + OH$
201	$H_2 + OH = H_2O + H$

Number	Reaction
202	$H_2 + O_2 = OH + OH$
203	$HO_2 + H = H_2 + O_2$
204	$HO_2 + H = OH + OH$
205	$HO_2 + O = OH + O_2$
206	$HO_2 + OH = H_2O + O_2$
207	$HO_2 + HO_2 = H_2O_2 + O_2$
208	$H_2O_2 + M = OH + OH + M$
209	$H_2O_2 + H = HO_2 + H_2$
210	$H_2O_2 + OH = H_2O + HO_2$
211	$O_3 + M = O_2 + O + M$
212	$O + O_3 = O_2 + O_2$
213	$OH + O_3 = HO_2 + O_2$
214	$HO_2 + O_3 = OH + O_2 + O_2$
215	$N + NO_2 = N_2O + O$
216	$N + NO_2 = NO + NO$
217	$N + N + M = N_2 + M$
218	$N + OH = NO + H$
219	$N + O + M = M + NO$
220	$N + O_2 = NO + O$
221	$N + O_3 = NO + O_2$
222	$N + NO = N_2 + O$
223	$ND2 + NO = N_2 + O$
224	$NP2 + NO = N_2 + O$
225	$ND2 + O_2 = NO + O$
226	$NP2 + O_2 = NO + O$
227	$N + N_2O = NO + N_2$
228	$ND2 + N_2O = NO + N_2$
229	$N + NO_2 = N_2O + O$
230	$N + NO_2 = NO + NO$
231	$ND2 + NO_2 = N_2O + O$
232	$ND2 + NO_2 = NO + NO$
233	$NP2 + NO_2 = N_2O + O$
234	$NP2 + NO_2 = NO + NO$
235	$N + H_2 = NH + H$
236	$NO + HO_2 = NO_2 + OH$
237	$NO + O + M = NO_2 + M$
238	$NO + OH + M = HNO_2 + M$
239	$HNO_2 + HNO_2 = NO + NO_2 + H_2O$
240	$NO + H + M = HNO + M$
241	$NO + NO_3 = NO_2 + NO_2$
242	$NO + O_3 = NO_2 + O_2$
243	$NO + NO + O_2 = NO_2 + NO_2$
244	$NO + NH = N_2O + H$
245	$NO_2 + H = OH + NO$
246	$NO_2 + O + M = NO_3 + M$
247	$NO_2 + O = NO + O_2$
248	$NO_2 + OH + M = HNO_3 + M$
249	$NO_2 + OH = HO_2 + NO$
250	$NO_2 + HO_2 + M = HO_2NO_2 + M$
251	$HO_2NO_2 = HO_2 + NO_2$
252	$NO_2 + O_3 = NO_3 + O_2$

Number	Reaction
253	$NO_2 + NO_3 = N_2O_5$
254	$NO_2 + H_2O_2 = NO + HO_2 + OH$
255	$O + NO_3 = O_2 + NO_2$
256	$NO_3 + NO_3 = NO_2 + NO_2 + O_2$
257	$N_2O_5 = NO_2 + NO_3$
258	$N_2O_5 + H_2O = HNO_3 + HNO_3$
259	$OH + N_2O = HNO + NO$
260	$H + HNO = H_2 + NO$
261	$OH + HNO = H_2O + NO$
262	$OH + HNO = H_2O + NO$
263	$OH + HNO_2 = NO_2 + H_2O$
264	$OH + HNO_3 = NO_3 + H_2O$
265	ND2 + M = N + M
266	NP2 + M = N + M

* Reactions 1–22 involve radiation.

! Reactions not involving ionic species occur in both the forward and backward directions.

Arkitektkopia AB, Bromma, 2021

SKB is responsible for managing spent nuclear fuel and radioactive waste produced by the Swedish nuclear power plants such that man and the environment are protected in the near and distant future.

skb.se